# DYNAMIC ANALYSIS OF FLOW IN TWO DIMENSIONAL CHANNEL

A THESIS SUBMITTED TO
THE GRADUATE SCHOOL OF NATURAL AND APPLIED SCIENCES
OF
MIDDLE EAST TECHNICAL UNIVERSITY

BY

ERJONA ENGİN

IN PARTIAL FULFILMENT OF THE REQUIREMENTS
FOR
THE DEGREE OF MASTER OF SCIENCE
IN
ENGINEERING SCIENCES

FEBRUARY 2008

Approval of the thesis:

**DYNAMIC ANALYSIS OF FLOW IN TWO DIMENSIONAL CHANNEL**

Submitted by **ERJONA ENGİN** in partial fulfilment of the requirements for the degree of **Master of Science** in **Engineering Sciences Department, Middle East Technical University** by,

Prof.Dr. Canan Özgen
Dean, Graduate School of **Natural and Applied Sciences** _____

Prof.Dr. Turgut Tokdemir
Head of Department, **Engineering Sciences** _____

Assoc.Prof.Dr. Hakan Işık Tarman
Supervisor, **Engineering Sciences Department ,METU** _____

**Examining Committee Members:**

Prof.Dr. Turgut Tokdemir
Engineering Sciences Department, METU _____

Assoc.Prof.Dr. Hakan Işık Tarman
Engineering Sciences Department, METU _____

Prof.Dr. Hasan Taşeli
Department of Mathematics, METU _____

Assist.Prof.Dr. Ferhat Akgül
Engineering Sciences Department, METU _____

Assist.Prof.Dr. Utku Kanoğlu
Engineering Sciences Department, METU _____

**Date:** 06/02/2008

**I hereby declare that all the information in this document has been obtained and presented in accordance with academic rules and ethical conduct. I also declare that, as required by these rules and conduct, I have fully cited and referenced all material and results that are not original to this work.**

Name, Last Name: Erjona ENGİN

Signature:

# ABSTRACT


DYNAMIC ANALYSIS OF FLOW IN TWO DIMENSIONAL CHANNEL

ENGİN, Erjona

M.S., Department of Engineering Sciences

Supervisor: Assoc. Prof. Dr. Hakan Işık TARMAN

February 2008, 59 pages

The Poiseuille Flow is the flow of a viscous incompressible fluid in a channel between two infinite parallel plates. The behaviour of flow is properly described by the well-known Navier-Stokes Equations. The fact that Navier-Stokes equations are partial differential equations makes their solution difficult. They can rarely be solved in closed form. On the other hand, numerical techniques can be applied successfully to the well-posed partial differential equations.

In the present study pseudo-spectral method is implemented to analyze the Poiseuille Flow. The pseudo-spectral method is a high-accuracy numerical modelling technique. It is an optimum choice for the Poiseuille flow analysis due to the flows simple geometry. The method makes use of Fourier Transform and by handling operations in the Fourier space reduces the difficulty in the solution. Fewer terms are required in a pseudo-spectral orthogonal expansion to achieve the same accuracy as a lower order method.

Karhunen-Loève (KL) decomposition is widely used in computational fluid dynamics to achieve reduced storage requirements or construction of relatively low-dimensional models. In this study the KL basis is extracted from the flow field obtained from the direct numerical simulation of the Poiseuille flow.

*Key words:* 2-D Poiseuille flow, direct numerical simulation, Pseudo-spectral methods, Karhunen-Loève decomposition

# ÖZ

## İKİ BOYUTLU KANALDA AKIŞIN DİNAMİK ANALİZİ

ENGİN, Erjona

Yüksek Lisans, Mühendislik Bilimleri Bölümü

Supervisor: Assoc. Prof. Dr. Hakan Işık TARMAN

Şubat 2008, 59 sayfa

Poiseuille Akışı iki sonsuz paralel plaka arasında viskoz sıkıştırılamaz bir akışkanın akışıdır. Bu akışın davranışı Navier – Stokes denklemleri tarafından gösterilebilmektedir. Navier-Stokes denklemerinin kısmi diferensiyel denklem olmalarından ötürü çözümlerini elde etmek zordur. Bu denklemlerin analitik çözümleri nadiren elde edilebilmektedir. Sayısal teknikler denklemlerin çözümünde yardımcı araç olarak kullanılmaktadır.

Bu çalışmada, Poiseuille Akışı analiz etmek için Sanki – Spektral Yöntemlerden faydalanılmıştır. Sanki – Spektral Yöntemler yüksek oranda dogruluk sağlayan sayısal modelleme yöntemidirler. Poiseuille Akışın basit geometrisinden dolayı, bu yöntemler optimum bir seçim olmaktadır. Bu yöntemler Fourier Dönuşümünü kullanmaktadır. İşlemlerin Fourier uzayında gerçekleşmeleri çözümü kolaylaştırır. Sanki-Spektral Yöntemlerde daha düşük seviyedeki metodlardan elde edilen doğluluğa ulaşmak için daha az terim gerekmektedir.

Karhunen-Loeve ayrıştırma yöntemi, hesaplamalı akışkanlar dinamiğinde, veri sıkıştırmak ve daha düşük boyutlu model oluşturmak için kullanılmaktadır. Bu çalışmada, KL tabanı, Poiseuille akışın direkt sayısal simülasyonundan elde edilmiştir. Bu araçlar kullanılarak Poiseuille akışın laminar akıştan türbülansa geçişi incelenmiştir.

*Anahtar Kelimeler:* Poiseuille Akışı, Direkt Sayısal Simulasyon, Sanki- Spektral Yöntemler, Karhunen-Loeve Ayrışma Yöntemi

*To My Grandfather*

# ACKNOWLEDGEMENTS

The author wishes to express her profound gratitude to Assoc. Prof. Dr. Hakan Işık Tarman for his sincere supervision, guidance, advice, criticism and encouragement in every stage of this study.

The author thanks Prof. Dr. Halil Önder whose trust and support helped her advance one step further in the fluid dynamics study.

The help of Cihan Yıldırım in using the Sun Systems is highly appreciated.

The author thanks to her husband H. Kürşat Engin for his trust, encouragement and help not only in every stage of her studies but also every difficulty faced each time.

The friendship of Pelin Uygur was a great support and a source of motivation.

Finally the author also would like to thank to her family for their trust and sincere support even being far away.

# TABLE OF CONTENTS

# CHAPTER 1

# INTRODUCTION

Turbulence is a flow regime characterized by chaotic, stochastic property changes. Turbulence occurs nearly everywhere in nature. Turbulence results in increased drag; decreased flow rate; increased noise; enhanced mixing and heat transfer. These may be desirable or not, so in order to be able to predict and control, understanding is important. Due to the nature of turbulence, the means used to understand laminar flow cannot be used to understand it. Turbulence is nonlinear, highly unsteady, rotational and 3D. All these make the understanding of the transition from laminar flow to turbulent flow crucial.

Hydrodynamic stability theory is concerned with the response of a laminar flow to a disturbance of small or moderate amplitude. If the flow returns to its original laminar state one defines the flow as stable, whereas if the disturbance grows and causes the laminar flow to change into a different state, one defines the flow as unstable. (Schmid and Henningson, 2001). The foundations of hydrodynamic stability are settled by the work of Helmholtz, Kelvin, Rayleigh and Reynolds. The incidence of turbulence was first recognized in relation to flows through straight pipes and channel: Hagen – Poiseuille flow and Poiseuille plane flow respectively. Reynolds (1880) studied the stability of a flow in a pipe by means of experiments and showed that the laminar flow breaks down when the dimensionless number Re, which after him is called the Reynolds number, exceeds a critical value, and that turbulence quickly ensues.

This study will focus on the Plane Channel Flow. Plane channel flow is also called Poiseuille flow after Jean Leonard Marie Poiseuille (Paris 1797-1869) due to his contribution in the study. The study of flow of liquids in small diameter glass capillaries is

one of the Poiseuille study topics. He considered the effects of pressure drop, tube length, tube diameter and temperature. Poiseuille together with Hagen empirically established the Hagen-Poiseuille Law:

$$Q = \frac{\pi \Delta P R^4}{8 \nu L}$$

The problem of Poiseuille Flow was solved by Stokes as an application of Navier-Stokes Equations. Plane channel flow is very adequate to study the dynamics of transition of the flow from laminar state to turbulent state. It is used to understand the no-slip boundary condition for a viscous flow at a solid boundary (Sutera and Skalak, 1993). This problem has been studied for years and some of the work to which is referred in this study is given as follows.

One of the main steps in understanding the stability of viscous flows was taken by Orr (1907) and Sommerfeld (1908), who derived the equation that now bears their name. The Orr-Sommerfeld equation arose from the research on the stability to infinitesimal disturbances in a linear approximation of plane Poiseuille flow. The first numerical solution of the Orr-Sommerfeld equation was obtained by Thomas (1953) trying to clarify the existing controversies concerning the existing asymptotic methods of approximation and confirming the instability of plane Poiseuille flow. Thomas (1953) used finite difference method to approximate the derivatives.

Lin (1955), Orszag (1971), Drazin and Reid (1982) studied further the equation. A critical Reynolds number $Re_{cr} = 5772.22$ for $\alpha = 1.02056$ was obtained by Orszag and Kells (1980). However experimental research performed by Carlson et al (1982), Nioshika and Ashai (1985) and Alavyoon et al (1986) have shown that transition for turbulence is observed for Re values as low as 1000. This incompatibility expands the research area. Due to Squire's (1933) theorem, to every three-dimensional perturbation of the linearized Navier-Stokes equations for a given Re and α, it corresponds a two dimensional perturbance for some $\widetilde{\alpha} \geq \alpha$ and $Re^* \leq Re$. Squire's theorem has been one of the main reasons of firstly focusing on the study and understanding of the two-dimensional behaviour. Some papers concerning finite amplitude solutions of Plane

Poiseuille flow in two and three dimensions that are taken as reference in this study are given as follows.

The first computational attempt was carried out by Noether (1921), who implemented Fourier series to expand equilibrium wave disturbances. Only one Fourier mode in the periodic direction is considered. Meksyns and Stuart (1951) solved simultaneously the Orr-Sommerfeld equation and a non-linear equation of mean motion, implementing asymptotic expansions, to find periodic solutions of finite amplitude. The results were $(\alpha, Re) \cong (1.20, 2900)$ and $(\tilde{\alpha}, Re^*) \cong (1.12,\ 5000)$.

Joseph and Sattinger (1972) expanded the flow , periodic in time and streamwise direction, as power series, and used Runge-Kutta integration on the resulting vorticity equations, Joseph and Sattinger (1972) showed that the only time-periodic solution which bifurcates from laminar Poiseuille flow is a two dimensional wave, which is unstable for the lowest Reynolds and small values of the amplitude. This instability makes perturbations of laminar flow snap through the unstable time-periodic flow to solutions of large amplitudes.

Zahn et al (1974) constructed a numerical integrator in space and time, using one and two Fourier modes in the streamwise coordinate in two-dimensions and just one mode in three-dimensions. The cross-stream variable was transformed to improve accuracy in boundary layers. The derivatives were approximated by means of finite differences. An implicit scheme is implemented in time discretization. The flow was driven by a constant mean pressure gradient. A surface of the energy of disturbances for each pair $(\alpha, Re)$ is obtained. An upper and a lower branch of solutions were received. These sets of solutions were perturbated and followed in time. The lower branch resulted unstable and the upper one stable for the tested disturbances.

Herbert (1976) employed a spectral method to approximate the vorticity equation for plane Poiseuille flow in two dimensions. He used Galerkin - Fourier with N ≤ 4 modes for the stream variable and Chebyshev and collocation-Chebyshev with K ≤ 64 modes. In order to obtain a finite system of algebraic equations, the solution was imposed to be a

periodic secondary flow with even or odd Fourier harmonics according to the parity of its order. The flow was driven by a constant mean pressure gradient. Neutral surface of periodic flow and the minimum value of $Re$ were found for the discretization. Fourier series resulted slowly convergent. Jimenez (1990) simplified full numerical simulation of spatially periodic channel with large longitudinal aspect ratios. Computations were performed using 41×85 Fourier-Chebyshev modes.

Casas and Jorba (2004) by means of a numerical integrator of the Navier-Stokes equations let the fluid evolve from an initially perturbed unstable solution until the fluid reaches an attracting state. The flow was driven either by a constant mean pressure gradient or by a constant flux. Different flow families were obtained.

# CHAPTER 2

# POISEUILLE FLOW

## 2.1 Definition

Poiseuille Flow is the flow of a viscous incompressible fluid in a channel between two infinite parallel plates. In this study, 2D Poiseuille Flow is considered. The flow behaviour is considered to be properly described by the Navier – Stokes Equations and incompressibility condition.

Navier – Stokes Equations are named after Claude Louis Navier and George Gabriel Stokes. The fluid studied is assumed to be a continuum, in other words, there is no abrupt change in its properties. The Navier – Stokes Equations are differential equations. They establish relations among the rate of changes of properties. They are established by combining the fluid kinematics and constitutive relation into the fluid equation of motion. These equations are extensions of the Euler Equations and include the effect of the viscosity in the flow. Navier – Stokes Equations are used to understand both compressible and incompressible fluid. So, in our case the incompressibility condition is applied,

$$\nabla \cdot \boldsymbol{u} = 0$$

$$\rho\left(\frac{\partial \boldsymbol{u}}{\partial t} + \boldsymbol{u} \cdot \nabla \boldsymbol{u}\right) + \nabla \boldsymbol{P} = k e_x + \mu \nabla^2 \boldsymbol{u}.$$

Here, $\nabla \cdot \boldsymbol{u}$ is the incompressibility condition, the term $\rho\left(\frac{\partial \boldsymbol{u}}{\partial t} + \boldsymbol{u} \cdot \nabla \boldsymbol{u}\right)$ describes inertia, $\frac{\partial \boldsymbol{u}}{\partial t}$ is the unsteady acceleration term and $\boldsymbol{u} \cdot \nabla \boldsymbol{u}$ the convective acceleration term. The

convective terms are nonlinear for incompressible Newtonian flow. On the other hand, $\nabla \boldsymbol{P}$ represents the pressure gradient and $\mu \nabla^2 \boldsymbol{u}$ represents the viscous term.

The flow geometry is mathematically defined as:

$$x \in R;\ y \in [-h, h];\ t > 0$$

where $x$ (or $x_1$) the streamwise variable and $y$ (or $x_2$) is the wall-normal variable. Similarly, $(u, v) = (u_1, u_2)$ denotes the streamwise and wall-normal velocity components, respectively. Non-slip boundary condition applies because of the finite fluid viscosity μ,

$$\boldsymbol{u}(x, -h, t) = \boldsymbol{u}(x, h, t) = 0.$$

Artificial boundaries are considered in the stream direction $x$. Let L be fixed period, then

$$\boldsymbol{u}(x, y, t) = \boldsymbol{u}(x + L, y, t).$$

There exist two different approaches in defining the driving force of the flow, either pressure gradient or flux. In this study, the flow is considered to be driven by a uniform pressure gradient $k$ in x – direction.

Fluid flow is assumed to be composed of mean flow and the fluctuations from the mean as

$$\boldsymbol{u} = \langle u_i \rangle + \boldsymbol{u}' \tag{2.1}$$

where $< u_i >$ defines the mean flow and $\boldsymbol{u}'$ defines the deviation from the mean flow.

The mean flow $\langle u_i \rangle = U(y)\delta_{i1}$, is given by

$$\langle u_i \rangle \equiv \lim_{T \to \infty} \frac{1}{T} \int_{-T/2}^{T/2} u_i(\boldsymbol{x}, \mathrm{t}) dt \equiv \lim_{L \to \infty} \frac{1}{T} \int_0^{\mathrm{L}} u_i(\boldsymbol{x}, \mathrm{t}) dx$$

where $L$ denotes the length of the channel. The last equivalence is a result of ergodicity assumption according to which, for sufficiently large $T$ and $L$ time averaging is equivalent to length averaging.

Substituting 2.1 into the NS equations, the fluctuation terms satisfies the following:

$$\rho\left\{\frac{\partial \boldsymbol{u}'}{\partial t}+\boldsymbol{u}'\cdot\nabla\boldsymbol{u}'\right\}+\frac{\partial p'}{\partial x_i}=-\rho\left\{U\frac{\partial \boldsymbol{u}'}{\partial x}+e_x\left(\boldsymbol{u}'\frac{\partial U}{\partial y}-\frac{\partial \boldsymbol{u}'}{\partial y}\right)\right\}+\mu\nabla^2\boldsymbol{u}$$

and the mean flow satisfies

$$k=-\frac{\partial}{\partial y}\left\{\mu\frac{\partial U}{\partial y}-\rho\langle u'v'\rangle\right\} \tag{2.2}$$

The uniform pressure gradient $k$ is balanced by the Reynolds stress ( $\rho\langle u'v'\rangle$) and the shear stress due to mean flow $\left(\mu\frac{\partial U}{\partial y}\right)$. The fluctuating component is driven by the interactions with the mean flow and the mean flow is driven by the constant uniform pressure gradient $k$. Integrating twice the equation of the mean

$$U(y)=\frac{1}{\nu}\int_{-h}^{y}\langle u'v'\rangle dy+\frac{kh}{\mu}\left(\frac{h^2-y^2}{2h}\right)$$

in the case of laminar flow

$$\frac{1}{\nu}\int_{-h}^{y}\langle u'v'\rangle dy=0$$

gives

$$U(y)=\frac{kh}{\mu}\left(\frac{h^2-y^2}{2h}\right) \tag{2.3}$$

Equation 2.3 gives the parabolic velocity profile.

The wall skin friction is:

$$\tau = \mu \frac{\partial U}{\partial y}\Big|_{y=-h} = kh.$$

Removing the primes, from now on, $\boldsymbol{u}$ defines the fluctuation velocities.

The friction velocity is defined as:

$$u_\tau = \sqrt{\tau/\rho} = \sqrt{kh/\rho}.$$

A wall length scale can be defined as:

$$l_\tau = \frac{\nu}{u_\tau}.$$

where $l_\tau$ and $u_\tau$ are micro scales associated with the boundary region, whereas the channel half height $h$, centreline velocity $u_{CL} = U(h)$, are macro scales associated with the core region.

Bulk velocity,

$$u_b = \frac{1}{2h}\int_{-h}^{h} U(y)dy$$

is another macro scale for velocity.

Performing normalization by implementing $u_\tau$ as scale for velocity, $h$ for length, $h/u_\tau$ for time

$$\frac{\boldsymbol{u}}{u_\tau} \to \boldsymbol{u}^* \; ; \; \frac{\boldsymbol{x}}{h} \to \boldsymbol{x}^* \; ; \; \frac{t}{h/u_\tau} \to t^* \; ; \; \frac{\rho}{\rho \, u_\tau^2} \to P^*.$$

The normalized *NS* equations will be

$$\nabla \cdot \boldsymbol{u}^* = 0$$

$$\frac{\partial \boldsymbol{u}^*}{\partial t} + \boldsymbol{u}^* \cdot \nabla \boldsymbol{u}^* + \nabla \boldsymbol{P} = \boldsymbol{e}_x + \frac{1}{Re} \nabla^2 \boldsymbol{u}^*$$

where the *Reynolds* number is:

$$Re = \frac{u_\tau h}{\nu} = \frac{h}{l_\tau}$$

Normalization is possible also using $l_\tau$ for the length scale. The resulting units after this normalization are called *wall units*. This normalization is given by:

$$\frac{\boldsymbol{u}}{u_\tau} \rightarrow \boldsymbol{u}^+ \; ; \; \frac{\boldsymbol{x}}{h} \rightarrow \boldsymbol{x}^+ \; ; \; \frac{t}{h/u_\tau} \rightarrow t^+.$$

The conversion between friction and wall units:

$$\boldsymbol{y}^+ = \frac{\mathrm{y}}{l_\tau} = \frac{yRe}{h} = y^* Re,$$

$$t^+ = t^* Re.$$

The wall units measure smaller scales in the near wall region and commonly called the micro units. The friction units are sometimes referred to as macro units. The next section gives somewhat more detailed information about the normalization.

## 2.2 Scales and normalizations

In this section, further details about the normalizing units used and the resulting normalized equations are explained.

Integrating the equation 2.2 once yields:

$$-\frac{ky}{\rho} = -\langle u'v' \rangle + \nu \frac{dU}{dy} - u_\tau^2 \tag{2.5}$$

where $u_\tau$ the friction velocity as is mentioned in the previous section. Substituting $\sqrt{kh/\rho}$ for $u_\tau$ in equation 2.5, we get:

$$u_\tau^2 \left(1 - \frac{y}{h}\right) = -\langle u'v' \rangle + \nu \frac{dU}{dy} \tag{2.6}$$

If $u_\tau$ and $h$ are utilized to normalize the equation the result is the following expression:

$$1 - \frac{y}{h} = -\frac{\langle u'v' \rangle}{u_\tau^2} + \frac{\nu}{u_\tau h} \frac{d(U/u_\tau)}{d(y/h)} \tag{2.7a}$$

Applying the normalized frictional units yields,

$$1 - y^* = -\frac{\langle u'v' \rangle}{u_\tau^2} + \frac{1}{Re} \frac{du^*}{dy^*} \tag{2.7b}$$

For large values of the friction *Reynolds* number ($Re = u_\tau h/\nu$), the viscous stress is suppressed by this normalized form. The stress at the wall is predominated by the viscosity. As a result, this normalization cannot be valid near the wall as $Re \to \infty$. In order to solve this problem, the second unit system (*wall units*) was presented in the preceding section.

Another normalized form is required in the immediate vicinity of the wall in order to handle the problem of vanishing viscosity due to large values of $Re$. This can be achieved by simply absorbing the friction *Reynolds* number in the length scale. With thus modification 2.6 becomes,

$$1 - \frac{y}{h} = -\frac{\langle u'v' \rangle}{u_\tau^2} + \frac{d(U/u_\tau)}{d(yu_\tau/\nu)} \tag{2.8a}$$

Employing the normalized wall units yields,

$$1 - \frac{y^+}{Re} = -\frac{\langle u'v' \rangle}{u_\tau^2} + \frac{du^+}{dy^+} \tag{2.8b}$$

The form stated in 2.8b tends to suppress the change of stress in the y-direction as $Re \to \infty$.

Let us reconsider 2.7b and 2.8b as $Re \to \infty$. Provided that $y^*$ remains $\mathcal{O}(1)$, 2.7b reduces to

$$1 - y^* = -\frac{\langle u'v' \rangle}{u_\tau^2} \tag{2.9}$$

This equation cannot be valid as $y^* \to 0$, which corresponds to finite values of $y^+$ (i.e. the vicinity of the wall). The part of the flow where 2.9 holds, is called the *core region*. 2.8b can be written as, $y^+$ being $\mathcal{O}(1)$,

$$1 = -\frac{\langle u'v' \rangle}{u_\tau^2} + \frac{du^+}{dy^+} \tag{2.10}$$

The above equation is not valid as $y^* \to \infty$ (the core region). The region of validity for 2.10 is called as the *surface layer*.

The two layer description (surface layer – core region) presented above requires a matching region. This matching should be done in a region characterized by the limits

$y^+ \to \infty$ and $y^* \to 0$. This can be achieved by a process known as asymptotic matching (Tennekes and Lumley, 1972). This overlap region of approximately constant *Reynolds* stress. The viscous stress on the other hand is very small compared to *Reynolds* stress in this region. Due to this lack of local viscous effects, this overlap region is called *inertial sublayer*. Since the stress at the surface is purely viscous in nature, as one moves down the inertial sublayer towards the wall there should be a region in which viscous stresses dominate over *Reynolds* stresses (this is also suggested by experimental evidence). This region is called the *viscous sublayer* and extends up to about $y^+ = 5$. The region where the viscous and inertial sublayers merge is called the *buffer layer*. In this region neither of the two stress components can be ignored. This layer is also the site for maximum turbulent energy production, which occurs approximately at $y^+ = 12$.

## 2.3 Linear Stability

We consider the linearized form of the governing equations for the fluctuations from the mean (eq.2.1),

$$\frac{\partial u}{\partial t} + U\frac{\partial u}{\partial x} + vU' = -\frac{\partial p}{\partial x} + \frac{1}{R}\nabla^2 u$$

$$\frac{\partial v}{\partial t} + U\frac{\partial u}{\partial x} \qquad = -\frac{\partial p}{\partial x} + \frac{1}{R}\nabla^2 v \tag{2.11}$$

where the primes on the fluctuating components are dropped and now a prime ($U'$) denotes a y-derivative. Here, we followed the convention and used a scaling based on the centerline velocity $u_{CL}$, thus $R = U_{CL}h/v$. This set of equations is completed by the continuity equation

$$\frac{\partial u}{\partial x} + \frac{\partial v}{\partial x} = 0. \tag{2.12}$$

Taking the divergence of the linearized momentum equations (2.11) and using the continuity equation (2.12) yields an equation for the fluctuations pressure:

$$\nabla^2 p = -2U' \frac{\partial v}{\partial x}.$$

This equation may be used with the second equation in (2.11) to eliminate $p$, resulting in an equation for the wall-normal velocity , $v$:

$$\left[\left(\frac{\partial}{\partial t} + U\frac{\partial}{\partial x}\right)\nabla^2 - U''\frac{\partial}{\partial x} - \frac{1}{R}\nabla^4\right] v = 0. \qquad (2.13)$$

The equation (2.13) is considered with the boundary conditions

$$v = v' = 0$$

at the walls.

Next, we introduce wavelike solutions of the form

$$v(x, y, t) = \hat{v}(y) e^{i(\alpha x - \omega t)}$$

where $\alpha$ denotes the streamwise wave number and $\omega$ stands for the frequency. Introducing this representation into (2.13) results in the following equation for $\hat{v}$

$$\left[(-i\omega + i\alpha U)(D^2 - \alpha^2) - i\alpha U'' - \frac{1}{R}(D^2 - \alpha^2)^2\right]\hat{v} = 0 \qquad (2.14)$$

with the boundary conditions $\hat{v} = D\hat{v} = 0$ at the walls. Here $D$ stands for the differentiation operator in the normal y-direction. This is the classical Orr-Sommerfeld equation [Drazin and Reid 1982, Schmid and Henningson 2001]. The frequency $\omega$ appears as the eigenvalue in the Orr-Sommerfeld equation, and together with the associated eigenfunctions $\hat{v}$ is generally complex. The spatial wave number $\alpha$ is assumed real. The critical Reynolds number is computed by Orszag to give $R_c = 5772.22$

corresponding to the wave number $\alpha = 1.02055$. This implies that for supercritical $R$ $(R > R_c)$, the flow is unstable to infinitesimal disturbances having the streamwise wave number $\alpha = 1.02055$, while for subcritical $R$ $(R < R_c)$, the flow is stable to infinitesimal disturbances (linearly stable).

It can be shown that the conventional Reynolds number ($R$) based on the centerline velocity $u_{CL}$, $R = u_{CL}h/\nu$, and the Reynolds number ($Re$) based on the friction velocity $u_\tau$, $Re = u_\tau h/\nu$, are related through

$$R = \frac{1}{2}Re^2 \tag{2.15}$$

in the regime of Poiseuille flow. Thus, $Re_c = \sqrt{2 \times 5772.22} = 107.4451$.

# CHAPTER 3

# DISCRETIZATION AND NUMERICAL SCHEME

Pseudo spectral methods are used to develop the numerical scheme implemented in the *FORTRAN* code. Pseudo spectral methods are chosen due to their high accuracy and fast convergence.

Reconsidering our equations in normalized form:

$$\nabla \cdot \boldsymbol{u} = 0$$

$$\frac{\partial \boldsymbol{u}}{\partial t} + \boldsymbol{u} \cdot \nabla \boldsymbol{u} = -\vec{\nabla} P + \boldsymbol{e_x} + \frac{1}{Re} \nabla^2 \boldsymbol{u}.$$

Recall $\omega = \nabla \times \mathrm{u}$ and $u \cdot \nabla u = \nabla(u \cdot u/2) - u \times \omega$. So,

$$\nabla \boldsymbol{u} = 0$$

$$\frac{\partial \boldsymbol{u}}{\partial t} = \boldsymbol{u} \times \boldsymbol{\omega} - \nabla \boldsymbol{\Pi} + \boldsymbol{e_x} + \frac{1}{Re} \nabla^2 \boldsymbol{u}$$

where $\nabla \boldsymbol{\Pi} = \mathrm{p} + \boldsymbol{u} \cdot \boldsymbol{u}/2$ is the dimensionless stagnation pressure (Guessous, 2003).

The boundary conditions are:

$u = v = 0$ at $\mathrm{y} = \pm 1$

## 3.1 Temporal Discretization

An implicit scheme is implemented in time integration. The non-linear terms are considered explicitly using Adams – Bashforth method. The pressure terms are discretized using an implicit Crank – Nicolson scheme. Both of the schemes are second order accurate in time. The resulting discretized equations are:

$$\nabla \cdot \boldsymbol{u}^{\mathrm{n}+1} = 0$$

$$\frac{\boldsymbol{u}^{\mathrm{n}+1} - \boldsymbol{u}^{\mathrm{n}}}{\Delta t} = \frac{3}{2}(\boldsymbol{u} \times \boldsymbol{\omega} + \mathbf{e}_{\mathrm{x}})^{\mathrm{n}} - \frac{1}{2}(\boldsymbol{u} \times \boldsymbol{\omega} + \mathbf{e}_{\mathrm{x}})^{\mathrm{n}-1} - \frac{1}{2}\nabla(\Pi^{\mathrm{n}+1} + \Pi^{\mathrm{n}}) + \frac{1}{Re}\frac{1}{2}\nabla^2(\boldsymbol{u}^{\mathrm{n}+1} + \boldsymbol{u}^{\mathrm{n}}).$$

They can be rearranged as:

$$\nabla \cdot \boldsymbol{u}^{\mathrm{n}+1} = 0 \tag{3.1}$$

$$\left(\frac{1}{Re}\nabla^2 - \frac{2}{\Delta t}\right)\boldsymbol{u}^{n+1} = \nabla\Pi^{\mathrm{n}+1} + \mathbf{g}^{\mathrm{n}} \tag{3.2}$$

where

$$\mathbf{g}^{\mathrm{n}} = -3\,(\boldsymbol{u} \times \boldsymbol{\omega} + \boldsymbol{e_x})^{\,n} + (\boldsymbol{u} \times \boldsymbol{\omega} + \boldsymbol{e_x})^{\,n-1} + \nabla\Pi^{\mathrm{n}} - \left(\frac{1}{Re}\nabla^2 - \frac{2}{\Delta t}\right)\boldsymbol{u}^{n}$$

and $\Delta t$ is the time step size.

The boundary conditions are $\boldsymbol{u}^{\mathrm{n}+1} = 0$ at $\boldsymbol{y} = \pm 1$ .

## 3.2 Spatial Discretization

In the definition of the problem, the flow geometry extends to infinity in the x-direction. In order to model the infinity in the $x$ - direction, periodicity is introduced. That was shown previously in the boundary conditions as

$$\boldsymbol{u}(x, y, t) = \boldsymbol{u}(x + L, y, t).$$

The result represents one spatial period of an infinite periodic pattern.

Assume that the flow takes place in the region of aspect ratio $s_x/2 \times 1$, where

$$0 \leq x \leq \frac{L}{h} = s_x \;\; ; \quad -1 \leq y \leq 1$$

$L$ is the dimensional length in $x$ - direction. Let $\xi = 2\pi/s_x$ be its wave number. Periodic boundary conditions are applied in the $x$ - direction with period $s_x = 2\pi/\xi$

$$\boldsymbol{u}\left(x + \frac{2\pi m}{\xi}, y, t\right) = \boldsymbol{u}(x, y, t) \qquad m \in Z^+.$$

The spatial discretization was accomplished using pseudo-spectral representations suggested by Orszag and Kells (1980) and Schumack et al (1991). Fourier series expansion of the dependent flow variables is used in the x-direction.

$$\begin{bmatrix} u \\ v \\ \prod \end{bmatrix}(x, y, t) = \sum_{|m|<\frac{M}{2}} \begin{bmatrix} \hat{u} \\ \hat{v} \\ \hat{\mathrm{P}} \end{bmatrix}(m, y, t) \times exp[i\, \xi_m\, x]$$

where the hats denote Fourier coefficients. The term $\xi_m = m\xi$ is the streamwise wave number and $m$ is the integer in the specified range.

The collocation points used in the x-direction are:

$$x_i = \frac{2\pi i}{\xi M} \;\; ; \;\; 0 \leq i \leq M.$$

In the $y$ – direction rescaled Legendre Lagrangian interpolant expansion is used for velocity and conventional Legendre polynomial expansion with order two less than that used for velocity is used for pressure (Schumack et al, 1991).

The lower order expansion for pressure eliminates the need to use a staggered grid in the solution and the problem of pressure boundary conditions that arise when Poisson equation is used to solve pressure. So,

$$\boldsymbol{u}(m,y,t) = \sum_{j=0}^{N} \overline{\boldsymbol{u}}(m,j,t)\bar{h}_j(y) \equiv \sum_{j=0}^{N} \overline{\boldsymbol{u}}_j h_j(y)$$

$$\boldsymbol{P}(m,y,t) = \sum_{j=1}^{N-1} \bar{P}(m,j,t)L_{j-1}(y) \equiv \sum_{j=1}^{N-1} \bar{P}_j L_{j-1}(y)$$

where $L_j(y)$ is the Legendre polynomial and $\bar{h}_j(y)$ is the rescaled Legendre Lagrangian polynomial of order j.

At the grid points, the rescaled Lagrangian interpolants satisfy:

$$\bar{h}_j(y_i) = \frac{1}{\sqrt{\omega_j}}\delta_{ij}$$

where $\delta_{ij}$ is the usual Kronecker's Delta function. The value of $\overline{\boldsymbol{u}}(m,j,t)$ computed by the numerical code is the rescaled value.

The Fourier coefficients at $y_i$ will be:

$$\widehat{\boldsymbol{u}}(m, y_i, t) = \bar{u}(m, y_i, t)\bar{h}_i(y_i) = \frac{\overline{\boldsymbol{u}}(m, y_i, t)}{\sqrt{\omega_i}}.$$

The pressure coefficients $\bar{P}(m, j, t)$ are the spectral coefficients of the Legendre polynomial of order j.

In order to convert the fields between the physical and Fourier Space representations, Fast Fourier Transformation (FFT) is typically used in pseudo-spectral methods. Non-linear terms involve difficult and time consuming convolution sums in spectral space. So, it is preferred performing the computation of nonlinear terms in physical space through simple multiplication at the grid points.

Horizontal derivatives are easily computed in the Fourier Space. The derivative of $e^{ikx}$ is $ike^{ikx}$. Except the non linear terms, Fourier representation is used for all the rest.

## 3.3 Numerical Scheme

The numerical scheme implemented in this study is based on the work of Patera (1984), Schumack (1991) and Guessous (2003). The algorithm makes use of the variational form of the governing equations. The modification of the "spectral method" (Patera, 1984) is applied in order to obtain a divergence free flow. This resolves the need of artificial pressure boundary conditions.

Let us consider the governing equations in terms of Fourier Coefficients

$$i\xi\hat{\mathrm{u}}^{n+1} + \frac{\partial\hat{\mathrm{v}}^{n+1}}{\partial y} = 0 \tag{3.3}$$

$$\left[\frac{1}{Re}\left(\frac{\partial^2}{\partial y^2} - \xi^2\right) - \frac{2}{\Delta t}\right]\hat{\mathrm{u}}^{n+1} = i\xi\hat{P}^{n+1} + \hat{g}_1^n \tag{3.4}$$

$$\left[\frac{1}{Re}\left(\frac{\partial^2}{\partial y^2}-\xi^2\right)-\frac{2}{\Delta t}\right]\hat{\mathrm{v}}^{n+1}=\frac{\partial \hat{P}^{n+1}}{\partial y}+\hat{g}_2^n \tag{3.5}$$

In order to discretize the problem a variational formulation is used. The inner product between the above equations in the y-direction and the same test function is taken.

These test functions are:

$$w_i(y)=\bar{h}_i(y)\ ,i=1,\dots,N-1$$

$$q_i(y)=L_{i-1}(y)\ ,i=1,\dots,N-1.$$

For $0<i<N$, $w_i$ ensures that the test functions of the governing equations satisfy the Dirichlet Boundary Condition of the problem,

$$w_i(\pm 1)=\bar{h}_i(\pm 1)=0.$$

The equations become

$$\int_{-1}^{1} q_i(y)\left[i\xi\hat{\mathrm{u}}^{n+1}+\frac{\partial \hat{\mathrm{v}}^{n+1}}{\partial y}\right]dy=0 \tag{3.6}$$

$$\int_{-1}^{1} w_i(y)\left[\frac{1}{Re}\left(\frac{\partial^2}{\partial y^2}-\xi^2\right)-\frac{2}{\Delta t}\right]\hat{\mathrm{u}}^{n+1}dy=\int_{-1}^{1} i\xi w_i(y)\hat{P}^{n+1}dy+\int_{-1}^{1} w_i(y)\hat{g}_1^n dy$$

(3.7)

$$\int_{-1}^{1} w_i(y)\left[\frac{1}{Re}\left(\frac{\partial^2}{\partial y^2}-\xi^2\right)-\frac{2}{\Delta t}\right]\hat{\mathrm{v}}^{n+1}dy=\int_{-1}^{1} w_i(y)\frac{\partial \hat{P}^{n+1}}{\partial y}dy+\int_{-1}^{1} w_i(y)\hat{g}_2^n dy$$

(3.8)

Integration by part is performed for the $\frac{\partial^2}{\partial y^2}$ and $\frac{\partial \hat{P}^{n+1}}{\partial y}$ terms

$$\int_{-1}^{1} w_i \frac{\partial^2 \hat{u}^{n+1}}{\partial y^2} dy = \left[ w_i \frac{\partial \hat{u}^{n+1}}{\partial y} \right]\Big|_{-1}^{1} - \int_{-1}^{1} \frac{dw_i}{dy} \frac{\partial \hat{u}^{n+1}}{\partial y} \, dy$$

$w_i \frac{\partial \hat{u}^{n+1}}{\partial y}\Big|_{-1}^{1} = 0$ → from Dirichlet Boundary Conditions

$$\Rightarrow \int_{-1}^{1} w_i \frac{\partial^2 \hat{u}^{n+1}}{\partial y^2} dy = - \int_{-1}^{1} \frac{dw_i}{dy} \frac{\partial \hat{u}^{n+1}}{\partial y} \, dy.$$

The pressure terms:

$$\int_{-1}^{1} w_i \frac{\partial \hat{P}^{n+1}}{\partial y} dy = \left[ w \hat{P}^{n+1} \right]\Big|_{-1}^{1} - \int_{-1}^{1} \frac{dw_i}{dy} \hat{P}^{n+1} \, dy$$

$\left[ w \hat{P}^{n+1} \right]\Big|_{-1}^{1} = 0$ ⟶ from Dirichlet Boundary Conditions

$$\Rightarrow \int_{-1}^{1} w_i \frac{\partial \hat{P}^{n+1}}{\partial y} dy = - \int_{-1}^{1} \frac{dw_i}{dy} \hat{P}^{n+1} \, dy.$$

Substituting into the governing equations:

$$\int_{-1}^{1} q_i(y) \left[ i\xi \hat{u}^{n+1} + \frac{\partial \hat{v}^{n+1}}{\partial y} \right] dy = 0 \tag{3.9}$$

$$\int_{-1}^{1} \frac{1}{Re} \frac{dw_i}{dy} \frac{\partial \hat{u}^{n+1}}{\partial y} dy - \left( \frac{\xi^2}{Re} + \frac{2}{\Delta t} \right) \int_{-1}^{1} w_i \frac{\partial \hat{u}^{n+1}}{\partial y} \, dy$$
$$= i\xi \int_{-1}^{1} w_i \hat{P}^{n+1} dy + \int_{-1}^{1} w_i \hat{g}_1^n dy \tag{3.10}$$

$$\int_{-1}^{1} \frac{1}{Re}\frac{dw_i}{dy}\frac{\partial \hat{\mathrm{v}}^{n+1}}{\partial y}dy - \left(\frac{\xi^2}{Re}+\frac{2}{\Delta t}\right)\int_{-1}^{1} w_i \frac{\partial \hat{\mathrm{v}}^{n+1}}{\partial y}\,dy$$
$$= -\int_{-1}^{1}\frac{dw_i}{dy}\hat{P}^{n+1}dy + \int_{-1}^{1} w_i \hat{g}_2^n dy \qquad (3.11)$$

Using the Einstein Summation notation

$$\mathbf{u}^{n+1} = \sum_{j=0}^{N} \overline{\mathbf{u}}_j^{n+1}\bar{h}_j = \overline{\mathbf{u}}_j^{n+1}\bar{h}_j$$

$$P^{n+1} = \sum_{j=1}^{N-1} \bar{P}_j^{n+1}\bar{L}_{j-1} = \bar{P}_j^{n+1}\bar{L}_{j-1}$$

with the boundary condition $\overline{\mathbf{u}}_0 = \overline{\mathbf{u}}_N = 0$, for every test function $w_i$ and $q_i$ where $1 \le i \le N-1$, equations 3.9, 3.10 and 3.11 will be

$$\int_{-1}^{1} L_{i-1}\left[i\xi\bar{h}_j\bar{\mathrm{u}}_j^{n+1} + \bar{h}_j'\hat{\mathrm{v}}^{n+1}\right]dy = 0 \qquad (3.12)$$

$$-\frac{1}{Re}\int_{-1}^{1}\bar{h}_i'\bar{h}_j'\bar{\mathrm{u}}_j^{n+1}dy - \left(\frac{\xi^2}{Re}+\frac{2}{\Delta t}\right)\int_{-1}^{1}\bar{h}_i\bar{h}_j\bar{\mathrm{u}}_j^{n+1}\,dy$$
$$= i\xi\int_{-1}^{1}\bar{h}_i\bar{L}_{j-1}\bar{P}_j^{n+1}dy + \int_{-1}^{1}\bar{h}_i\bar{h}_j\bar{g}_{1j}^n dy \qquad (3.13)$$

$$-\frac{1}{Re}\int_{-1}^{1}\bar{h}_i'\bar{h}_j'\bar{\mathrm{v}}_j^{n+1}dy - \left(\frac{\xi^2}{Re}+\frac{2}{\Delta t}\right)\int_{-1}^{1}\bar{h}_i\bar{h}_j\bar{\mathrm{v}}_j^{n+1}\,dy$$
$$= -\int_{-1}^{1}\bar{h}_i\bar{L}_{j-1}\bar{P}_j^{n+1}dy + \int_{-1}^{1}\bar{h}_i\bar{h}_j\bar{g}_{2j}^n dy \qquad (3.14)$$

where the primes denotes derivative with respect to $y$.

The integrals are evaluated making use of the Gauss-Lobato Quadrature with the weighting functions

$$w_j = \frac{2}{N(N+1)\left[L_N(y_j)\right]^2}.$$

Recall that $\bar{h}_j(y_i) = \delta_{ij}/\sqrt{w_j}$. The integrals become:

$$\int_{-1}^{1} \bar{h}_i \bar{h}_j \, dy = \sum_{p=0}^{N} w_p \bar{h}_i(y_p) \bar{h}_j(y_p) = \delta_{ij} = B_{ij} \tag{3.15}$$

$$\int_{-1}^{1} \bar{h}_i' \bar{h}_j' \, dy = \sum_{p=0}^{N} w_p \bar{h}_i'(y_p) \bar{h}_j'(y_p) = A_{ij} \tag{3.16}$$

$$\int_{-1}^{1} \bar{h}_i \bar{L}_{j-1} \, dy = \sum_{p=0}^{N} w_p \bar{h}_i(y_p) \bar{L}_{j-1}(y_p) = \sqrt{w_j} L_{j-1}(y_i) = D_{ij} \tag{3.17}$$

$$\int_{-1}^{1} \bar{h}_i' L_{j-1} \, dy = \sum_{p=0}^{N} w_p \bar{h}_i'(y_p) L_{j-1}(y_p) = \mathcal{D}_{ij} \tag{3.18}$$

Note that the Einstein Summation Convention does not apply in the above equations.

In order to obtain the derivatives of the rescaled Lagrangian interpolants, the derivatives for standard Legendre Lagrangian interpolants (Gottlieb et al, 1979) are modified.

$$\bar{h}_j'(y_j) = \begin{cases} \dfrac{1}{\sqrt{w_j}} \dfrac{L_N(y_i)}{L_N(y_i)(y_i - y_j)}, & i \neq j \\ 0, & i = j \neq 0, N \\ -\alpha/4\sqrt{w_j}, & i = j = 0 \\ +\alpha/4\sqrt{w_j}, & i = j = N \end{cases}$$

where $\alpha = N(N+1)$.

Legendre Basis and rescaled Legendre Lagrangian interpolation is used to represent velocity due to their computational efficiency for a weak formulation, even though Chebyshev and Lagrange expansion methods have similar accuracies (Ronquist and Patera, 1987). This is due to the natural selection of unity weighting in the inner products for a Legendre Basis. Legendre Polynomials are orthogonal relative to a weight function of one.

Gauss-Lobatto quadrature is defined relative to the weight function of the orthogonal set of polynomials (Canuto et al 1988). If $P(y)$ is a polynomial of order less or equal to $2N-1$, then

$$\int_{-1}^{1} P(y)w(y)dy = \sum_{j=0}^{N} P(y_j)w_j.$$

The inner products of the Legendre-based method are defined with weight one, similar to Gauss-Lobatto quadrature. Usage of Legendre-Gauss Lobatto grid point in the y-direction and Lagrangian interpolants for the velocities seriously simplifies the sums in the equations 3.15 – 3.18. This would not have been possible if Chebyshev polynomials had been used. So, this choice apparently decreases the operation count.

Let us rescale the interpolants as done in 3.15 – 3.18. The matrix $[B_{ij}]$will become the identity matrix. This solves the problem of rescaling the data before analysis. The governing equations become

$$i\xi D_{ji}\bar{\mathrm{u}}_j^{n+1} + \mathcal{D}_{ji}\bar{\mathrm{v}}_j^{n+1} = 0 \tag{3.19}$$

$$-\frac{1}{Re}A_{ij}\bar{\mathrm{u}}_j^{n+1} - \left(\frac{\xi^2}{Re} + \frac{2}{\Delta t}\right)B_{ij}\bar{\mathrm{u}}_j^{n+1} = i\xi D_{ij}\bar{P}_j^{n+1} + B_{ij}\bar{g}_{1j}^{n} \tag{3.20}$$

$$-\frac{1}{Re}A_{ij}\bar{\mathrm{v}}_j^{n+1}-\left(\frac{\xi^2}{Re}+\frac{2}{\Delta t}\right)B_{ij}\bar{\mathrm{v}}_j^{n+1}=-\mathcal{D}_{ij}\bar{P}_j^{n+1}+B_{ij}\bar{g}_{2j}^{n} \qquad (3.21)$$

In the matrix form $A_{ij}, B_{ij}, D_{ij}, \mathcal{D}_{ij}$are the elements of $(N-1)\times(N-1)$ sized $\underline{A}, \underline{B}, \underline{D}, \underline{\mathcal{D}}$ matrices.

For every wave number $\xi, \underline{\mathrm{u}}^{n+1}, \underline{\mathrm{v}}^{n+1}, \underline{\bar{P}}^{n+1}$represents the vector array of length $(N-1)$ constructed of elements $\bar{\mathrm{u}}_j^{n+1}, \bar{\mathrm{v}}_j^{n+1}, \bar{P}_j^{n+1}$ where $1 \le j \le N-1$

If discrete Helmholtz operation is defined as

$$\underline{H}=-\left(\frac{1}{Re}\underline{A}+\left(\frac{\xi^2}{Re}+\frac{2}{\Delta t}\right)\underline{I}\right)$$

and the superscript T represents the transpose term, for every $\xi$

$$i\xi\underline{D}^T\underline{\mathrm{u}}^{n+1}+\underline{\mathcal{D}}\,\underline{\mathrm{v}}^{n+1}=0 \qquad (3.22)$$

$$\underline{H}\,\underline{\mathrm{u}}^{n+1}=i\xi\underline{D}\,\underline{\bar{P}}^{n+1}+\underline{\bar{g}}_1^{n} \qquad (3.23)$$

$$\underline{H}\,\underline{\mathrm{v}}^{n+1}=-\underline{\mathcal{D}}\,\underline{\bar{P}}^{n+1}+\underline{\bar{g}}_2^{n} \qquad (3.24)$$

And the boundary conditions are $\bar{\mathrm{u}}_0=\bar{\mathrm{u}}_N=0$.

To solve the equations, firstly they are divided into two sets, for velocity and pressure according to Uzawa Method (Canuto, 1993). For velocity components:

$$\underline{\mathrm{u}}^{n+1}=\underline{H}^{-1}(\,i\xi\underline{D}\,\underline{\bar{P}}^{n+1}+\underline{\bar{g}}_1^{n}) \qquad (3.25)$$

$$\underline{\mathrm{v}}^{n+1}=\underline{H}^{-1}(\,-\underline{\mathcal{D}}\,\underline{\bar{P}}^{n+1}+\underline{\bar{g}}_2^{n}) \qquad (3.26)$$

For pressure we insert the above equations into the continuity equation 3.22 to obtain a discrete equation

$$\underline{S_t}\,\bar{\underline{P}}^{n+1} = -i\xi\underline{D}^T\,\underline{H}^{-1}\bar{\underline{g}}_1^n - \underline{\mathcal{D}}\,\underline{H}^{-1}\bar{\underline{g}}_2^n$$

where $\underline{S_t} = -(\xi^2\underline{D}^T\,\underline{H}^{-1}\underline{D} + \underline{D}^T\,\underline{H}^{-1}\underline{\mathcal{D}})$ is the discrete pressure operator.

The equation can be solved for pressure $\bar{\underline{P}}^{n+1}$ for every wave number $\xi$. The result will be substituted into 3.25 and 3.26, and solved for velocity components.

To avoid spurious pressure mode problems, the constant pressure mode is set to zero (Schumack et al, 1991)

$$\bar{P}_1 = 0 \quad \text{at} \quad \xi^2 = 0$$

for which the pressure operator matrix is modified as

$$\underline{S_t} = \begin{bmatrix} 1 & 0 & \cdots & 0 \\ 0 & & & \\ \vdots & & [\![\underline{S_t}_{ij}]\!] & \\ 0 & & & \end{bmatrix} \quad \text{if} \quad \xi^2 = 0.$$

## 3.4 Velocity Solvers

In order to solve for the velocities in x and y direction at each time step, a matrix equation must be solved in each direction for every wave number $\xi$. Multiply the right hand side of the equation 3.25 and 3.26 by the inverse of $H(\underline{H}^{-1})$.

$$\underline{H}^{-1}\cdot\underline{H}\,\bar{\underline{\mathrm{u}}}^{n+1} = \underline{H}^{-1}i\xi\underline{D}\,\bar{\underline{P}}^{n+1} + \bar{\underline{g}}_1^n$$

$$\underline{H}^{-1}\cdot\underline{H}\,\bar{\underline{\mathrm{v}}}^{n+1} = -\underline{H}^{-1}\underline{\mathcal{D}}\,\bar{\underline{P}}^{n+1} + \bar{\underline{g}}_2^n$$

$H$ is a full $(N-1)\times(N-1)$ matrix. The inversion is performed using the collocation diagonalization method (Haidvogel and Zang, 1979) made possible by the rescaled Lagrangian interpolants that lead to a mass identity matrix.

Making use of this method reduces the computational cost of matrix inversion to $O(N^2)$. $\underline{A}$ is the symmetric second order $y-$ derivative matrix that can be diagonalized as $\underline{A}=\underline{E}\,\underline{G}\,\underline{E}^{-1}$ where $\underline{G}$ is a diagonal matrix whose elements are the eigenvalues of $\underline{A}$. $\underline{E}$ is a matrix composed of the eigenvectors of $\underline{E}$ and $\underline{E}^{-1}$ is its inverse.

Consider the Helmholtz operator $H$ for a given wave number $\xi$ in terms of $A$.

$$\underline{H}=-\left(\frac{1}{Re}\underline{E}\,\underline{G}\,\underline{E}^{-1}+\left(\frac{\xi^2}{Re}+\frac{2}{\Delta t}\right)\underline{I}\right) \tag{3.27}$$

Multiply by $\underline{E}^{-1}$

$$\underline{E}^{-1}\underline{H}=-\left(\frac{1}{Re}\underline{G}+\left(\frac{\xi^2}{Re}+\frac{2}{\Delta t}\right)\underline{I}\right)\underline{E}^{-1}=-\underline{\mathcal{G}}\underline{E}^{-1}\,.$$

Multiply both sides by $\underline{\mathcal{G}}^{-1}$ then by $\underline{E}$

$$-\underline{E}^{-1}\underline{\mathcal{G}}^{-1}\underline{E}^{-1}\underline{H}=\underline{I}\,.$$

The inverse of $\underline{H}$ is obtained as:

$$\underline{H}^{-1}=-\underline{E}^{-1}\left(\frac{1}{Re}\underline{G}+\left(\frac{\xi^2}{Re}+\frac{2}{\Delta t}\right)\underline{I}\right)^{-1}\underline{E}^{-1}\,.$$

This inverting $H$ reduces to inverting the diagonal matrix $\mathcal{G}$. Notice that the presence of the identity matrix is what makes the simple factorization of 3.27 possible.

# CHAPTER 4

# KARHUNEN – LOÈVE DECOMPOSITION

## 4.1 Karhunen – Loève (KL) Decomposition

The KL expansion is the representation of a vector field $u(x,t)$ as a series of the form:

$$u = \sum_{n=1}^{\infty} a_n(t)\phi^n(x).$$

In terms of an orthonormal set of functions $\phi^{(n)}$,

$$\left(\phi^{(n)}, \phi^{(m)}\right)_x = \int_V \phi_j^{(n)}\phi_j^{(m)}dV = \delta_{nm} \quad \text{where } j = 1,2.$$

Summation convention on repeated indices $(\cdot,\cdot)_x$ denotes inner product over $x$. The time dependent coefficients $a_n$ are required to satisfy

$$E\{a_{n,}a_m\} = \int a_n(t)a_m(t)dt = \lambda_n\delta_{nm}$$

where $E\{\}$ indicates the ensemble average. For any truncated representation

$$u^N = \sum_{n=1}^{N} a_n(t)\phi^{(n)}(x)$$

the ensemble average is a maximum

$$E^N = \sum_{n=1}^{N} \lambda_n \, .$$

The orthonormal basis is set by functions $\phi^{(n)}$ such that they are eigenfunctions of

$$\int_V k_{ij}(x,x')\phi_j^{(n)}(x')dx' = \lambda_n \, \phi_i^{(n)}(x) \tag{4.1}$$

The kernel $k_{ij}$ is the autocorrelation tensor of the field $u$

$$k_{ij}(x,x') = E\{ u_i(x,t), u_j(x',t)\}.$$

The autocorrelation tensor is hermitian, non-negative and square integrable assures that a uniform convergent spectral representation for it exists (Mercer's Theorem (Riesz and Nagy, 1955)). So it is guaranteed that we have a complete set of orthonormal vector eigenfunctions $\phi^{(n)}$ as solutions to 4.1.

Since in the numerical formulation, the flow is assumed L-periodic in the x direction, the KL eigenfunctions take the form

$$\phi_j^{(n)}(x,y) = \hat{\phi}_j^{(n)}(m,y)\mathrm{e}^{-i\frac{2\pi m x}{L}}. \tag{4.2}$$

This, in turn, implies that the dependence of the KL eigenfunctions on the vertical variable y can be obtained by solving

$$\int_{-1}^{1} \widehat{K}_{ij}(m,y,y')\hat{\phi}_j^{(n)}(m,y')dy' = \lambda_n \hat{\phi}_j^{(n)}(m,y) \tag{4.3}$$

for each $|m| < M/2$ where $K_{ij}(m,y,y') = E\{\hat{u}_i(m,y,t), \hat{u}_j(m,y',t)\}$.

In order to increase the sharpness of the ensemble averaging procedure, the flow field ensemble is enlarged by introducing new admissible flow fields constructed from the computed flow field using symmetries of the governing equations. The continuous symmetry of translational invariance in the streamwise $x$ direction already leads to the complex exponential representation (4.2) of the KL eigenfunctions in the $x$ variable. The discrete symmetry in the vertical midplane,

$$\mathbf{F}\{\mathbf{u}\} = (\mathrm{u}_1(x,-y,t), -\mathrm{u}_2(x,-y,t))$$

is admissible and it leads to doubling the size of the original ensemble. Note that the symmetry operators $\mathbf{I}$ and $\mathbf{F}$ form a group of two elements $\{\mathbf{I},\mathbf{F}\}$ with $\mathbf{I} = \mathbf{F^2}$ the identity operator. Further, using the reality of the flow, we have

$$\hat{\mathbf{u}}(-m,y,t) = \overline{\hat{\mathbf{u}}}(m,y,t)$$

where overbar denotes complex conjugation. Thus, (4.3) needs to be solved for only $0 \le m < M/2$.

Since the computed flow field uses the Legendre basis and the corresponding Gaussian quadrature in the wall-normal direction, the integral equation can be discretized to get a matrix eigenvalue problem of size $2(N+1)$

$$\mathrm{K}\Phi = \lambda\Phi$$

where $\mathrm{K} = E\{\mathrm{V}(t) \otimes \mathrm{V}(t)\}$ and

$$\Phi = \left[\hat{\phi}_1(\mathrm{y}_0) \quad \cdots \quad \hat{\phi}_1(\mathrm{y}_\mathrm{N}) \quad \hat{\phi}_2(\mathrm{y}_0) \quad \cdots \quad \hat{\phi}_2(\mathrm{y}_\mathrm{N})\ \right]^\mathrm{T} \qquad \text{with}$$

$$\mathrm{V} = \left[\sqrt{\omega_0}\,\hat{\mathrm{u}}_1(\mathrm{y}_0) \quad \cdots \quad \sqrt{\omega_\mathrm{N}}\,\hat{\mathrm{u}}_1(\mathrm{y}_\mathrm{N}) \quad \sqrt{\omega_0}\,\hat{\mathrm{u}}_2(\mathrm{y}_0) \quad \cdots \quad \sqrt{\omega_\mathrm{N}}\,\hat{\mathrm{u}}_2(\mathrm{y}_\mathrm{N})\ \right]^\mathrm{T}.$$

Here, $\otimes$ denotes the dyadic product, $\hat{\mathrm{u}}_\mathrm{i}(\mathrm{y_j}) \equiv \hat{\mathrm{u}}_\mathrm{i}(m,\mathrm{y}_j,t)$ and $\hat{\phi}_\mathrm{i}(\mathrm{y_j}) \equiv \hat{\phi}_\mathrm{i}(\mathrm{m},\mathrm{y_j})$.

# CHAPTER 5

# RESULTS AND DISCUSSION

In this work, the numerical simulation is used to explore the stability and transition behavior of the 2D Poisseuille flow. The method of study is based on the numerical integration of the Navier Stokes equations for the time evolution of a disturbance flow field added upon the laminar parabolic base flow profile

$$U(y) = \frac{Re}{2}(1 - y^2).$$

The initial energy of the disturbance field is specified and the time evolution of the energy is monitored for growth or decay as indication of the stability of the base flow against the disturbances of specified initial magnitude of energy. Throughout these runs the simulation parameters are chosen as $M = 8$, $N = 70$ and the period $s = L/h = 2\pi/1.02056$ selected from literature. This corresponds to the critical wavenumber from the linear stability analysis (see section 2.3).

The disturbance flow field should itself be an admissible flow field, satisfying the spatial constraints such as the boundary conditions and the continuity equation as well as it should contain a rich mixture of the dynamical features of the flow in order to test the stability of the base flow against all possible type disturbances. In order to construct such a disturbance flow field, we performed the numerical simulation of the 2D channel flow at $Re = 200$ at which the resulting flow exhibits a dynamically rich nature. The resulting flow regime is depicted in Figure 5.1.

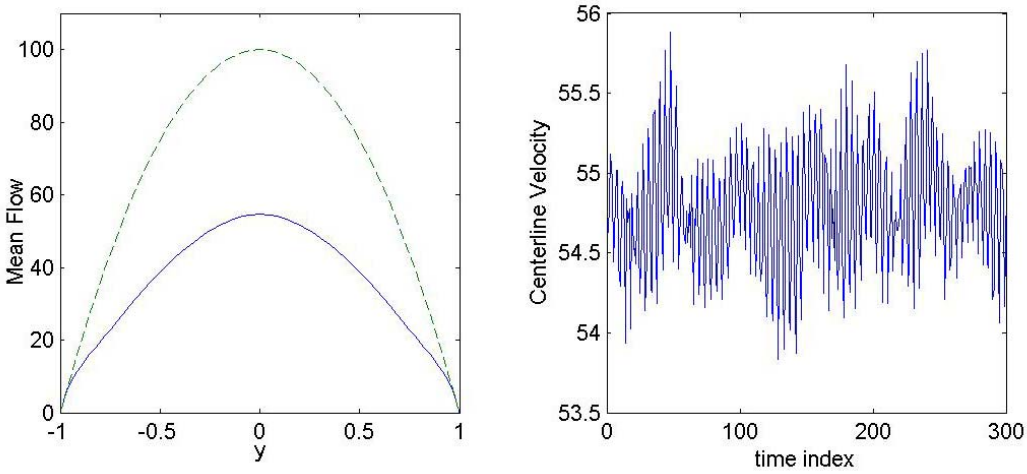


**Figure 5.1** The actual (solid) and laminar (dashed) mean parabolic profiles and the centerline velocity time series.

Clearly, at this high Re, the actual mean profile deviates from the corresponding laminar profile in such a way that the core region is getting flatter and the flow is getting retarded. This is a consequence of enhanced mixing between the two regions where the slow fluid in the wall region mixes with the fast fluid in the core region, thus an overall deceleration results.

KL decomposition is a tool for extracting the dynamical features contained in a database representing a flow field. Based on their contribution to the flow energy, it also reveals the hierarchy of these features which is specific to the flow regime under consideration. These features and their hierarchy are represented by the KL eigenvectors and the corresponding KL eigenvalues, respectively. The flow database at $Re = 200$ is used to generate the KL eigenpairs. Table 5.1 shows the first 10 KL eigenvalues as they are ordered and scaled with the magnitude of the largest eigenvalue.

It should be noted that the KL basis is generated using the fluctuating component of the flow field after the removal of the mean flow. Otherwise, the first basis element associated with the mean flow, namely $(m = 0,\ q = 1)$, would dominate in the energy content. The sharp drop in the energy content of the basis elements in the list as indicated by the corresponding eigenvalues shows the optimality of the decomposition

as the flow energy carried by the truncated representation of the flow in terms of KL modes, $u \approx u^N = \sum_{n=1}^{N} a_n \phi_n$ is maximal.

**Table 5.1** KL eigenvalues

| $Re = 200$ | | |
|---|---|---|
| $n$ | $m\ q$ | $\lambda_k/\lambda_l$ |
| 1 | 1 1 | 0.10e+1 |
| 2 | 2 1 | 0.14e-1 |
| 3 | 2 2 | 0.53e-2 |
| 4 | 3 1 | 0.29e-2 |
| 5 | 0 1 | 0.14e-2 |
| 6 | 1 2 | 0.13e-2 |
| 7 | 3 2 | 0.95e-3 |
| 8 | 0 2 | 0.82e-3 |
| 9 | 2 3 | 0.44e-3 |
| 10 | 2 4 | 0.28e-3 |

The vertical profiles of the corresponding KL eigenfunctions are shown in Figure 5.2.

As a result of the symmetry considerations in the construction of the covariance kernel, the KL eigenfunctions possess odd or even symmetry in the mid-plane. They satisfy the divergence-free property and the boundary conditions, so they are the building blocks of the underlying flow. They exhibit increased zero crossings as the index (wavenumber) increases, reminiscent of Sturm-Liouville type eigenfunctions. Some exhibit increased variation in the core region and some in the wall region that may invoke the classification as the core or the wall type to be utilized in the analysis of the underlying flow dynamics.

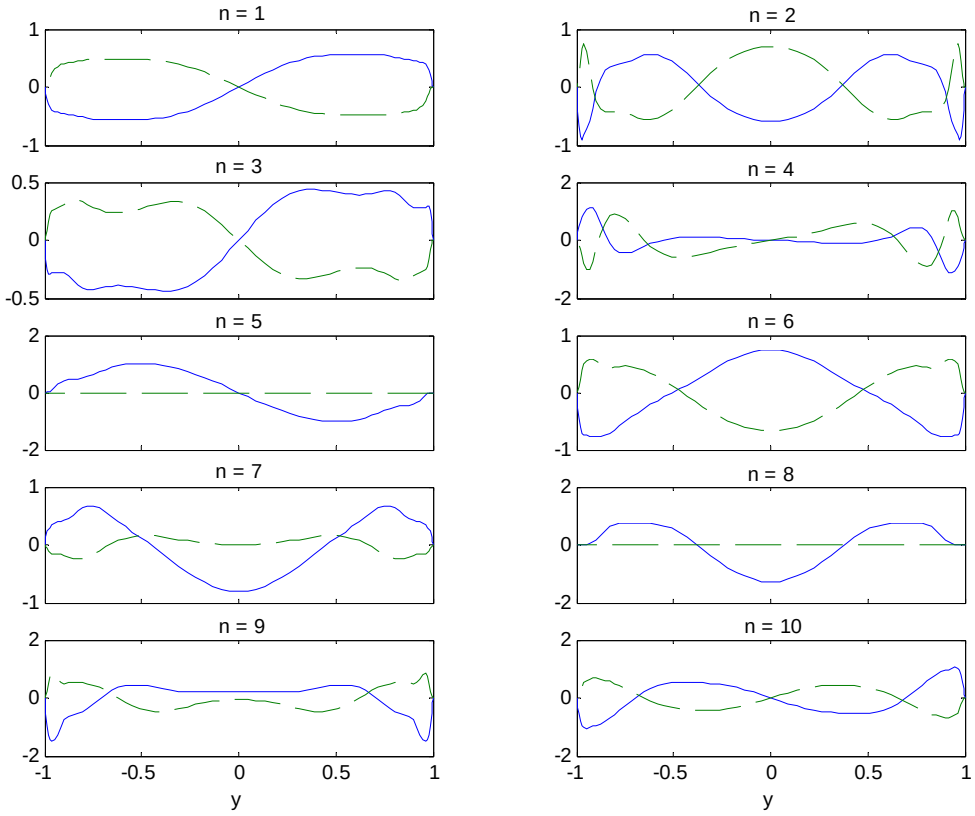


**Figure 5.2 The vertical profiles of the corresponding KL eigenfunctions.**

Time variation of the corresponding expansion coefficients, $a_n(t)$, and the KL spectrum are shown in Figure 5.3. This is obtained by projecting the fluctuating flow field at $Re = 200$ onto the KL basis, $a_n(t) = (\boldsymbol{u}(x,t), \boldsymbol{\phi}_n(x))$.

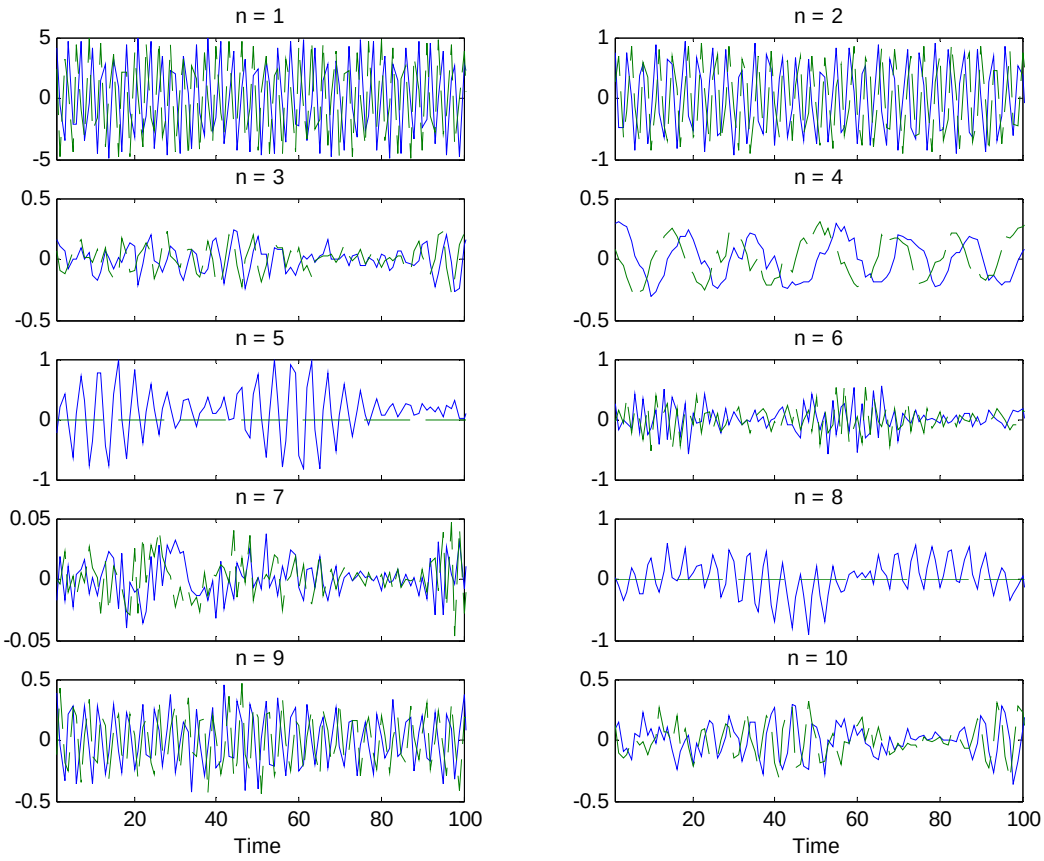


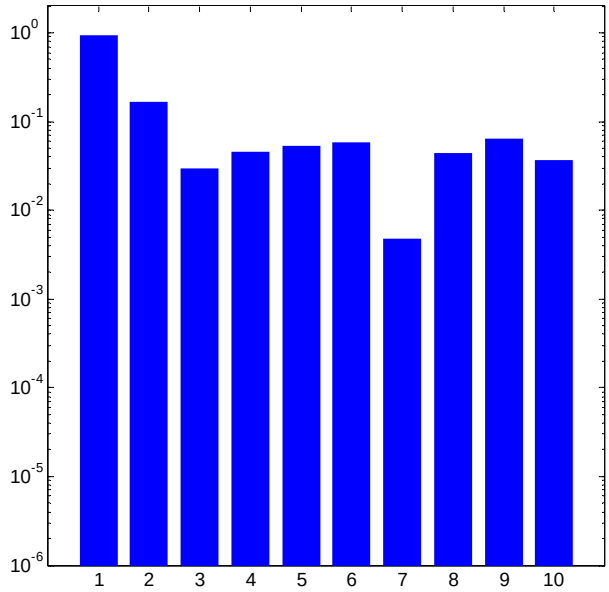

**Figure 5.3** The time variation of the projections of the flow field at $Re = 200$ onto the space spanned by the first 10 KL eigenfunctions of Table 5.1 and the corresponding KL spectrum, $\langle a_n \bar{a}_n \rangle^{1/2}$.

We will use this dynamically rich and parametrized flow field at $Re = 200$ to disturb the laminar base flow. For this purpose, the flow field at $Re = 200$ is reconstructed using a truncated KL representation containing only the most energetic KL modes. Normally, the appearance of each mode in the reconstruction is weighted by the corresponding KL eigenvalues

$$u \approx u^N = \sum_{n=1}^{N} \mathrm{a}_n(t)\phi_n(x,y) \;\; with \; \langle \mathrm{a}_{\boldsymbol{n}} \bar{\mathrm{a}}_{\boldsymbol{n}} \rangle = \lambda_n.$$

This is a weighting specific to the flow regime $Re = 200$. In the reconstruction of the flow field as a disturbance field, however, each KL mode is allowed to contribute equally to specified flow energy in order to provide an equal representation of dynamical features in the disturbance field. This specified flow energy is then used to control the energy level of the disturbance.

The energy of a flow field $\mathbf{u}$ is defined as

$$E(\mathbf{u}) = \frac{1}{2} \int_0^s \int_{-1}^{1} \mathbf{u} \cdot \bar{\mathbf{u}} \, dy \, dx,$$

thus, for the Poiseuille flow $E_P = E(U) = sRe/6$ . The energy of the disturbance flow field is normalized with respect to the basic quantity $E_P$ leading to the relative energy of the disturbance

$$\varepsilon(\mathbf{u}) = \frac{E(\mathbf{u})}{E_P}.$$

The disturbance field is then constructed as

$$\mathbf{u_0^N}(x,y) = A_0 \sum_{n=1}^{N} real\left(\boldsymbol{\varphi}^{(n)}(x,y)\right) \tag{5.1}$$

where $\boldsymbol{\varphi}^{(n)}(x,y) = \widehat{\boldsymbol{\varphi}}^{(n)}(m,y)e^{i2\pi mx/s}$ with $n = (m,q)$ and $A_0$ is a real constant such that $\varepsilon(\mathbf{u_0^N}) = \varepsilon_0$ . The evolution of the initial condition (5.1) for different initial energies $\varepsilon_0$ is computed at different $Re$ values. The truncation cut-off index is selected as $N = 50$ to achieve a level of dynamical richness in the initial disturbance field. The time evolution of the initial disturbance field for various initial energy and $Re$ values are shown in Figure 5.4.

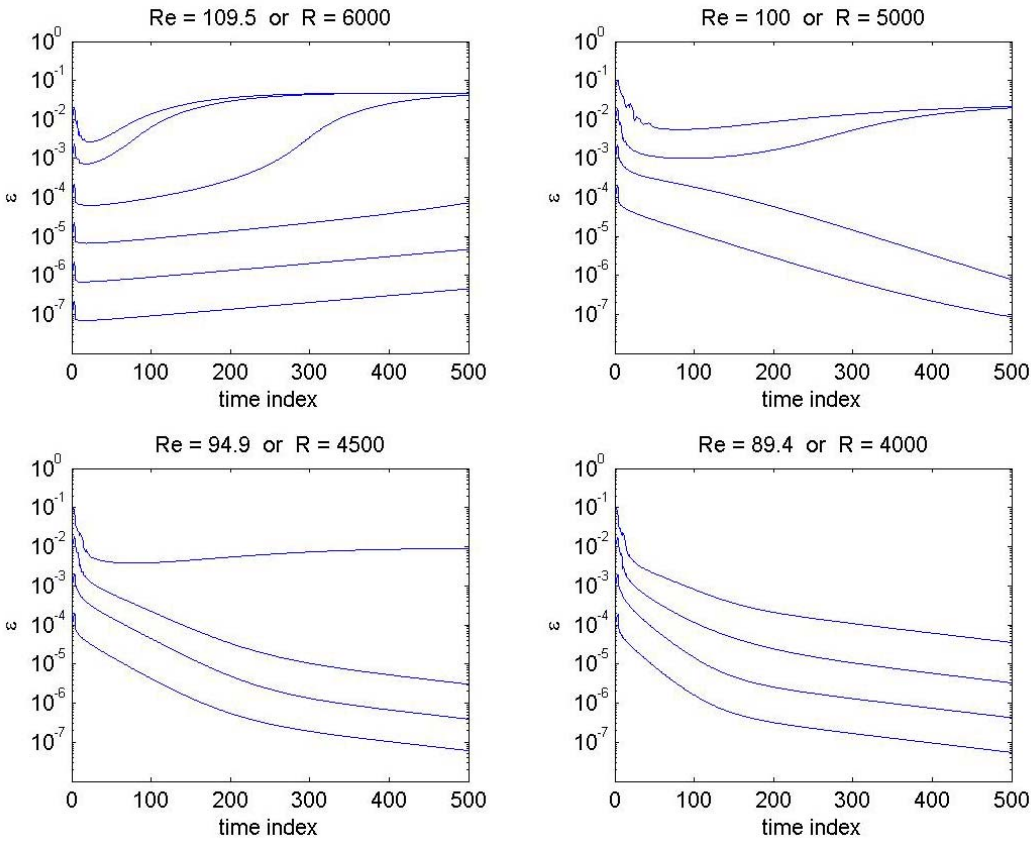


**Figure 5.4** The time evolution of the energy of the disturbances superimposed upon the base flow for various initial energy $\varepsilon_0$ and $Re$ values.

At the supercritical value of $\boldsymbol{R = 6000}(R > \boldsymbol{R_c})$, as expected and as a verification of our computations, the disturbances at all levels of initial energy experience growth. This is the region where the base flow is theoretically known to be unstable to infinitesimal disturbances (linearly unstable). At the subcritical $R$ values $(R < \boldsymbol{R_c})$ where it is theoretically known that the base flow is stable to infinitesimal disturbances (linearly

stable), we observe instability to finite disturbances (subcritical instability). Due to the instability of the base flow, the disturbances are attracted to another solution. The basin of attraction of this solution is sketched in Figure 5.5 crudely showing the threshold disturbance energy increasing with decreasing $Re$.

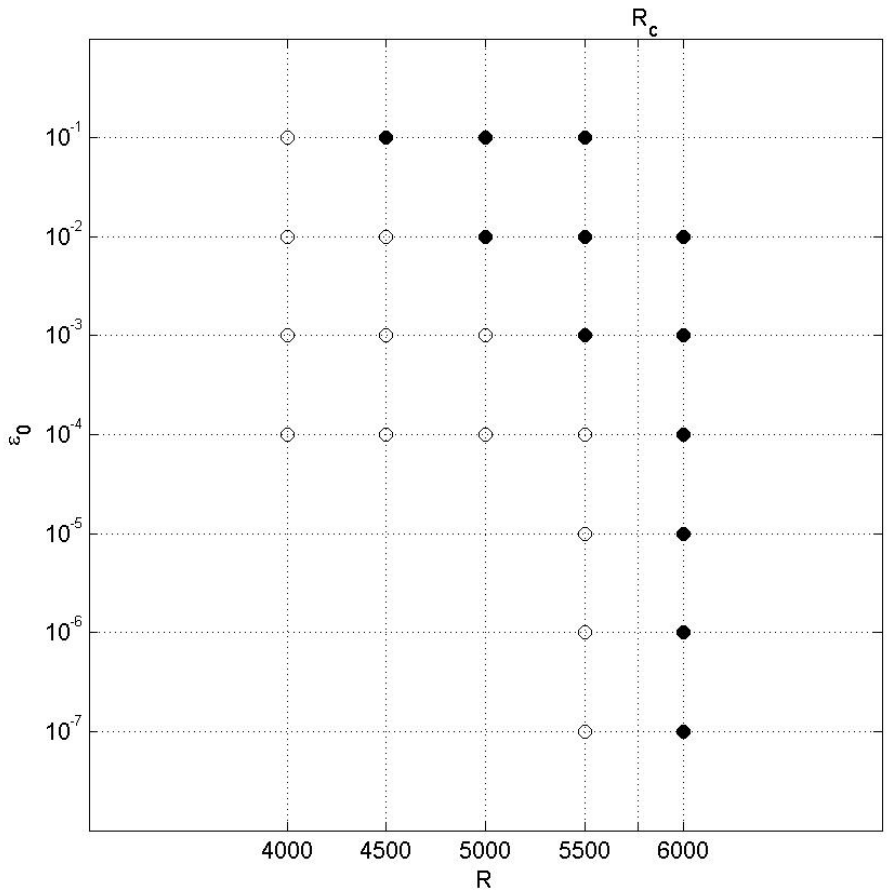


**Figure 5.5** The overall depiction of the instability of the disturbances of Figure 5.4 as stable (empty circle) and unstable (solid circle).

As shown in Figure 5.4, in the case of instability of the base flow, the disturbance field eventually converges to a new flow field. In the following series of figures, the projection of this flow field onto the first 10 the KL basis elements in Figure 5.2 as obtained at $Re = 200$ are shown.

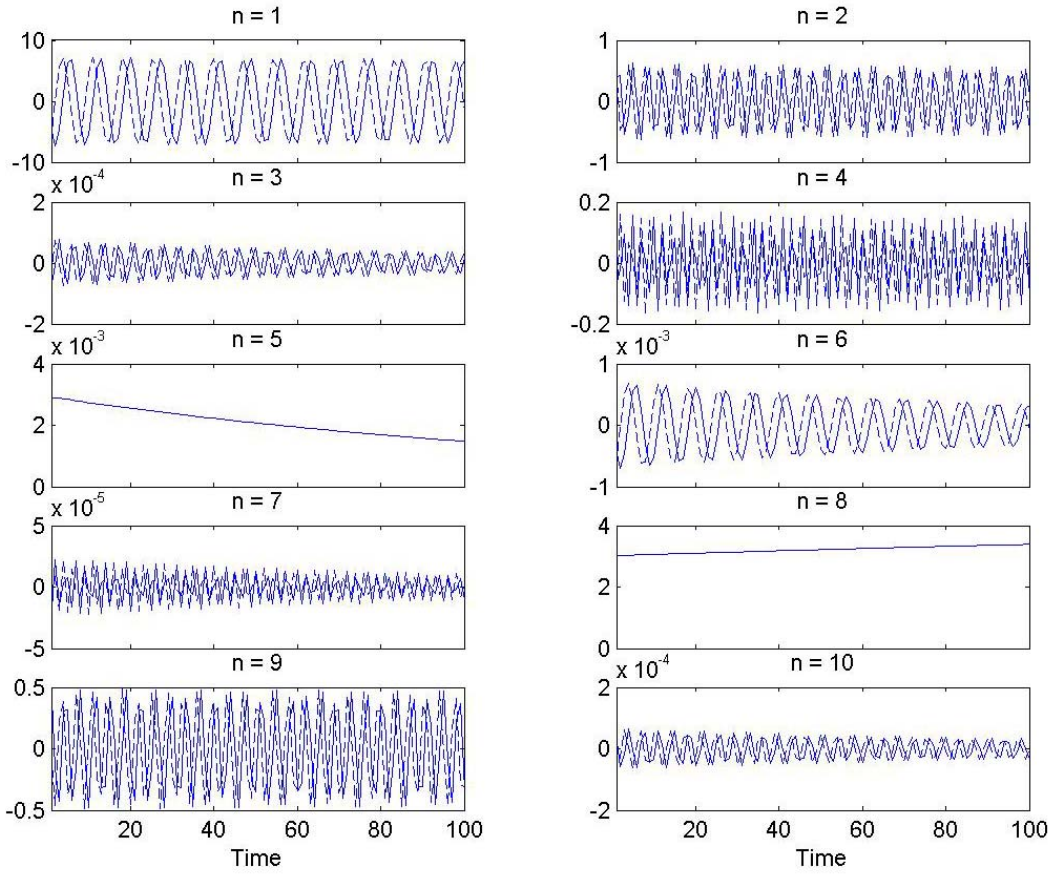


**Figure 5.6** The time variation of the projections of the limiting flow field obtained at $R = 6000$ in Figure 5.4 onto the space spanned by the first 10 KL eigenfunctions of Table 5.1.

Figure 5.6 indicates that the flow field obtained at supercritical $R = \mathbf{6000}$ is of periodic character as far as the most energetic component, namely $n = 1$, is concerned. The most striking behaviour are observed at $R = 55\mathbf{00}$ and $R = 4500$ in Figures 5.7 and 5.9, respectively, where the flow exhibits a quasi-periodic character unlike the periodic character at $R = 5\mathbf{000}$ in Figure 5.8, again as far as the most energetic component is concerned. These variations in the flow character in the subcritical regime call for a careful analysis as a future work.

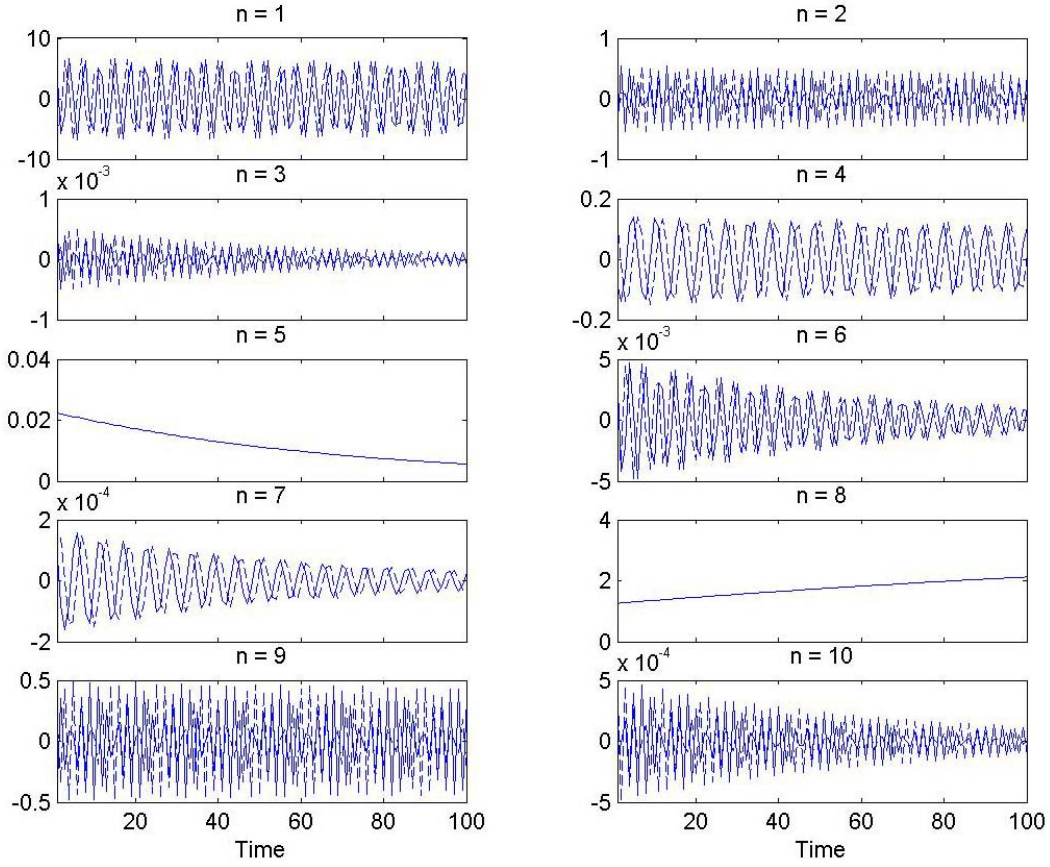


**Figure 5.7** The same as in Figure 5.6 at $R = 5500$.

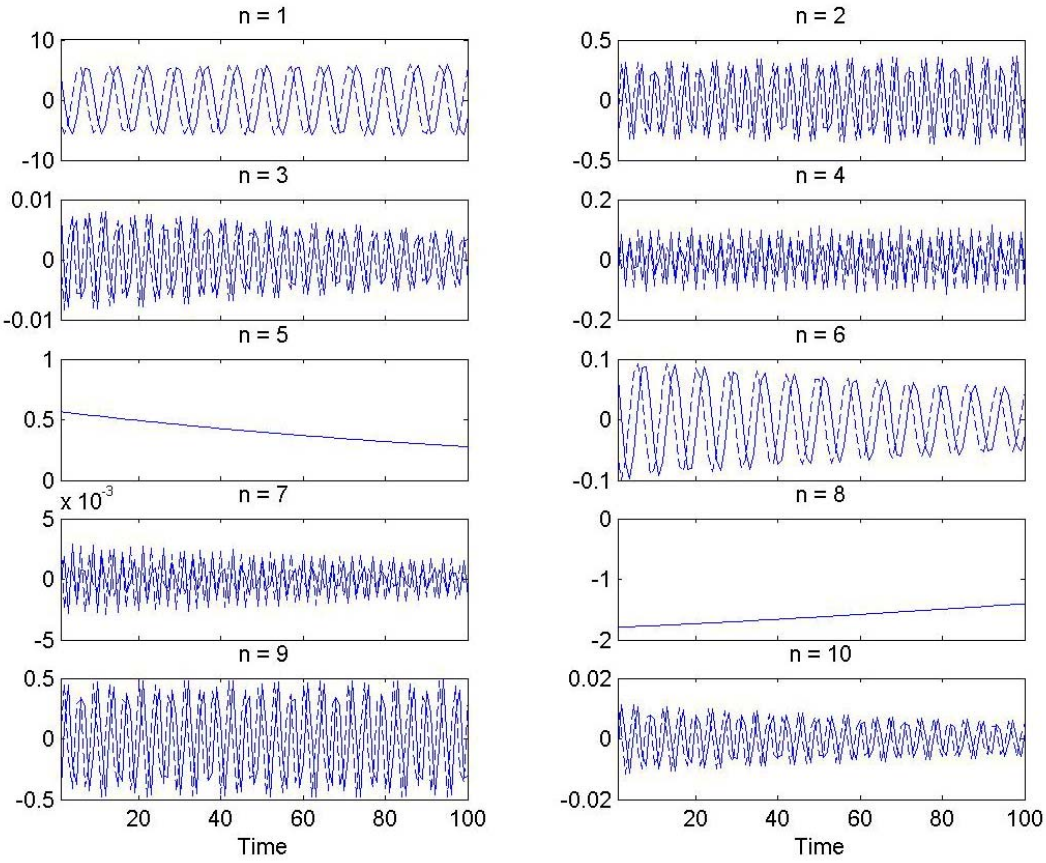


**Figure 5.8** The same as in Figure 5.6 at $R = 5000$.

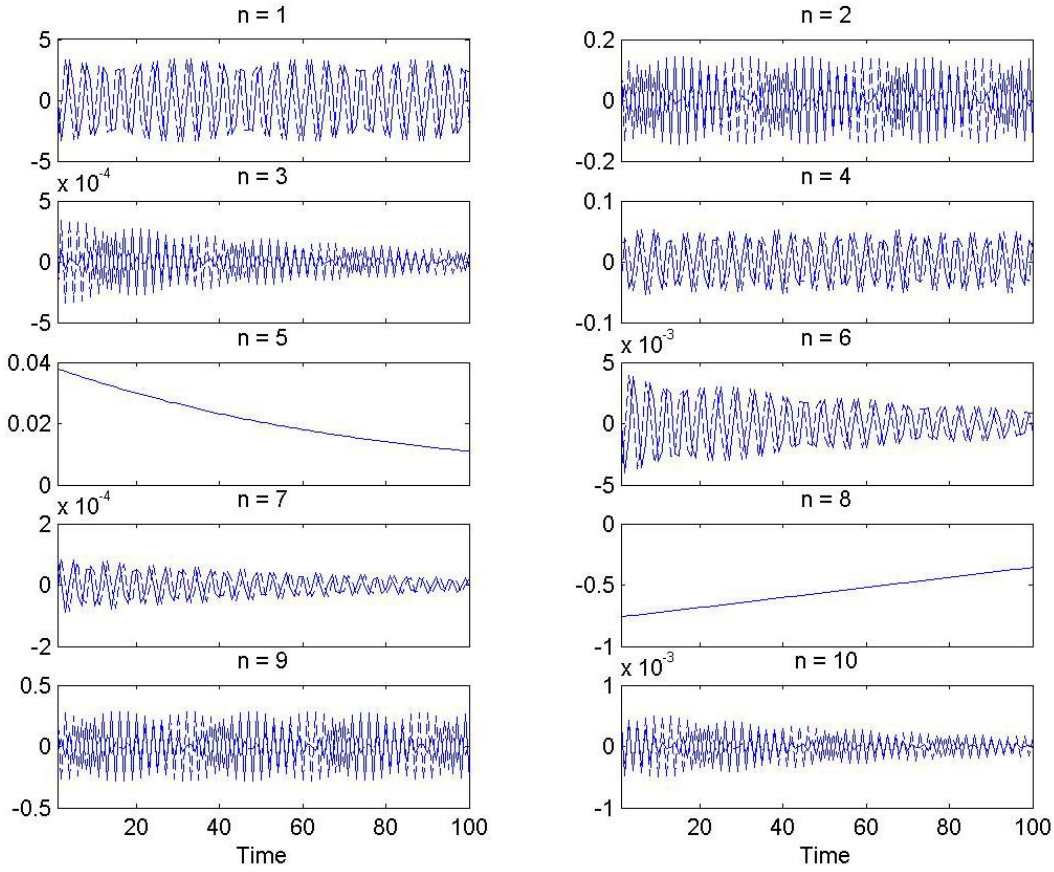


**Figure 5.9** The same as in Figure 5.6 at $R = 4500$.

# CHAPTER 6

# FUTURE WORK

In this work, KL basis is used to analyze the underlying dynamics in a passive sense as a parametrization of the projection space. Alternatively, KL basis can be used to construct a low dimensional description of the underlying phenomena using Galerkin procedure. In order to describe the procedure, considering the Navier-Stokes equations in the symbolic form

$$\frac{\partial \mathbf{u}}{\partial \mathrm{t}} = \mathrm{L}(\mathbf{u}, Re).$$

Where L represents the nonlinear differential operator involving **u**, spatial derivatives of **u**, and parameter Re. A low dimensional model capturing some important aspects of the governing equation may be constructed by projecting the original equation onto a KL subspace spanned by the Truncated KL expansion (via Galerkin projection). This can be done as follows: first the KL eigenfunctions are extracted from the field **u**, obtained by, say numerical simulation, at a reference value $Re_0$. The truncated expansion $\mathrm{u} \approx \mathrm{u}^{\mathrm{N}} = \sum_{\mathrm{n}=1}^{\mathrm{N}} \mathrm{a}_{\mathrm{n}}(\mathrm{t})\, \phi_{\mathrm{n}}(\mathrm{x})$ is then substituted into the original equation, resulting in a residue whose projection onto the KL subspace is zeroed

$$\left( \frac{\partial \mathbf{u}_{\mathrm{N}}}{\partial \mathrm{t}} = \mathrm{L}(\mathbf{u}_{\mathrm{N}}, \mathrm{Re}), \phi_{\mathrm{n}}(\mathbf{x}) \right) = 0.$$

This results in an amplitude equation of the form

$$\frac{\mathrm{da}_{\mathrm{n}}}{\mathrm{dt}} = \tilde{\mathrm{L}}(\mathrm{a}, Re)$$

For the KL expansion coefficients $\mathrm{a_n}$. This equation can be used to determine the time evolution of the expansion coefficients and thus may constitute a low dimensional model for the original equation in the neighbourhood of $Re_0$. Note that optimality of the KL expansion is no longer available when used for off reference values of $Re$, however, the KL expansion functions still satisfy all the spatial constraints of the flow field, such as boundary conditions, incompressibility conditions, etc.

# REFERENCES


Alavyoon, F., Henningson, D.S. and Alfredsson, P.H. (1986). Turbulent Spots in Plane Poiseuille Flow-Flow Visualition. *Physics of Fluids , 29*, 1328-1331.

Boyd, J. (1989). *Chebyshev and Fourier Spectral Methods.* Verlag: Springer.

Canuto, C. (1993). Spectral methods for viscous, incompressible flows. In H. K. Hussaini (Ed.), *Algorithmic Trends in Computational Fluid Dynamics* (pp. 169-193). Verlag (New York): Springer.

Canuto, C., Hussaini, M.Y., Quarteroni, A. and Zang, T.A. (1988). *Spectral Methods in Fluid Dynamics.* Verlag: Springer.

Carlson, D.R., Widnallm S.E. and Peeters, M.F. (1982). A Flow Visualization Study of Transition in Plane Poiseuille Flow. *Journal of Fluid Mechanics , 121*, 487-505.

Casas, P.S. and Jorba, A. (2004). Unstable Manifold Computations for the Two-Dimensional Plane Poisueille Flow. *Theoretical and Computaional Fluid Dynamics , 18*, 285-299.

Drazin, P.G. and Reid, W.H. (1982). *Hydrodynamic Stability.* Cambridge: Cambridge University Press.

Fortin, A., Jardak, M, Gervais, J.J. and Pierre, R. (1994). Old and New Results on the Two-Dimensional Poiseuille Flow. *Journal of Computational Physics , 115*, 455-469.

Gottlieb, D., Hussaini, M.Y. and Orszag S.A. (1984). Theory and application of spectral methods. In R. G. Voigt (Ed.), *Spectral Methods for Partial Differential Equations* (pp. 1-54). Philadelphia: SIAM.

Guessous, L. (2003). A Pseudo - Spectral Numerical Scheme for the Stimulation of Steady and Oscillating Wall - Bounded Flows. *Numer. Heat Trasf. (Part B) , 45*, 567-586.

Haidvogel, D.B and Zang, T. (1979). The Accurate Solution of Poisson's Equation by Expansion. *Journal of Computational Physics , 30*, 167-180.

Herbert, T. (1976). Periodic Secondary Motions in a Plane Channel. *Proc.5th Int. Conf. on Numerical Methods in Fluid Dynamics, Lecture Notes in Physics. 59*, s. 235-240. Springer.

Jimenez, J. (1990). Transition to turbulence in two-dimensional Poiseuille Flow. *Journal of Fluid Mechanics , 218*, 265-297.

Joseph, D.D. and Sattinger, D.H. (1972). Bifurcating Time Periodic Solutions and Their Stability. *Archive for Rational Mechanics and Analysis , 45*, 79-109.

Lin, C. (1955). *The Theory of Hydrodynamic Stability.* Cambridge: Cambridge University Press.

Maday, Y., Meiron, S., Patera, A.T. and Ronquist, E.M. (1993). Analysis of Iterative Methods for the Steady and Unsteady Stokes Problem: Application to Spectral Element Discretizations. *SIAM Journal of Scientific and Statistical Computing , 14* (2), 310-337.

Meksyn, D. and Stuart, J.T. (1951). Stability of Viscous Motion Between Parallel Planes for Finite Disturbences. *Proceedings of Royal Society of London*, *208 (Series A)*, pp. 517-526.

Nishioka, M. and Asai, M. (1985). Some Observations of the Subcritical Transition in Plane Poiseuille Flow. *Journal of Fluid Mechanics , 150*, 441-450.

Noether, F. (1921). Das Turbulenzproblem. *Z. Angew. Math. Mech.* (1), 125-138 and 218-219.

Orr, W. The Stability or Instability of the Steady Motions of a Perfect Liquid and of a Viscous Liquid. *Proceedings of Royal Irish Academy*, *27*, pp. 9-68 and 69-138.

Orszag, S. A. and Kells, L.C. (1980). Transition to turbulence in Plane Poiseuille flow and plane Couette flow. *Journal of Fluid Mechanics , 96*, 159.

Orszag, S. (1971). Accurate Solution of the Orr-Sommerfeld Stability Equation. *Journal of Fluid Mechanics , 50* (4), 689-703.

Patera, A. (1984). A Spectral Element Method for Fluid Dynamics: Laminar Flow in a Channel Expansion. *Journal of Comp. Physics , 54*, 468-488.

Poiseuille, J. (1840). Recherches Experimentelles sur le Mouvement des Liquides dans les Tubes de Tres Petit Diametres. *Comptes Rendus Acad. Sci.*, *11*, pp. 961-967 and 1041-1048.

Riesz, F. and Nagy, B.Z. (1955). *Functional Analysis.* New York: Unger.

Ronquist, E.M and Patera, A.T. (1987). A Legendre Spectral Element Method for the Stefan Problem. *International Journal for Numerical Methods in Engineering , 24* (12), 2273 - 2299.

Schmid, P.J. and Henningson, D.S. (2001). *Stability and Transition in Shear Flows* (Vol. 142). Verlag: Springer.

Schumack, M.R., Schultz, W.W. and Boyd, J.P. (1991). Spectral Method Solution of the Stokes Equations on nonstaggered grids. *Journal of Computational Physics , 94*, 30-58.

Squire, H. (1933). On the Stability of the Three-Dimensional Disturbances of Viscous Flow Between Parallel Walls. *Proceedings of the Royal Society of London* (Series A), 621-628.

Sutera, S.P. and Skalak, R. (1993). The History of Poiseuille's Law. *Annual Review of Fluid Mechanics , 25*, 1-19.

Tennekes, H. and Lumley, J.L. (1972). *A First Course in Turbulence.* The MIT Press.

Thomas, L. (1953). The Stability of Plane Poiseuille Flow. *Physical Review , 91* (4), 780 - 783.

Tuğluk, O. and Tarman, I. H. (2006). Dynamics of Wall-Bounded Flow. In K. T. Taş (Ed.), *Proc. International Symposium on Mathematical Methods in Engineering* (pp. 243-253). Ankara: Springer Netherlands.

Zahn, J.-P., Toomre, J., Spiegel, E.A. and Gough, D.O. (1974). Nonlinear Cellular Motions in Poiseuille Channel Flow. *Journal of Fluid Mechanics , 64*, 319-345.

# APPENDIX

# The Karhunen-Loève (KL) Process

## 1. The Eigenvalue Problem

The K-L decomposition or proper orthogonal decomposition is a technique to parameterize experimental or numerical data optimally in energy norm. The original data in this analysis is a set of two dimensional velocity vectors $v_i^n v_{\mathrm{i}}^n(\mathrm{x}_1, \mathrm{x}_2)$ where n denotes the moment in time, $i$ denotes the direction of the vector, and $\mathrm{x}_1, \mathrm{x}_2$ denotes the independent spatial variables. Although $vv$ must be real since it represents a physical velocity field, this analysis is done for a complex vector for reasons which will become obvious. The purpose of the *K-L method* is to identify a vector $\psi_i \psi_i \psi(\mathrm{x}_1, \mathrm{x}_2)$ which will maximize the quantity

$$\sum_n |\mathbf{v}^n \mathbf{v}^{\mathbf{n}}, \boldsymbol{\psi}\boldsymbol{\psi}|^2$$

subject to $(\boldsymbol{\psi}\boldsymbol{\psi}, \boldsymbol{\psi}\boldsymbol{\psi}) = 1$. With the inner product defined as

$$(a, b) = \int_D \overline{a}_i(\boldsymbol{x}) b_i(\boldsymbol{x}) d\boldsymbol{x} \qquad (\mathrm{A}.1)$$

where overbar indicates complex conjugation and summation on $i$ is assumed, and the energy defined as $|\boldsymbol{v}|^2 = (\boldsymbol{v}, \boldsymbol{v})^2$, the energy composed in the eigenfunction is measured by

$$E = \sum_{n=1}^{N} (\boldsymbol{v}^n, \boldsymbol{\psi})^2 = \sum_{n=1}^{N} (\boldsymbol{\psi}, \boldsymbol{v})(\boldsymbol{v}, \boldsymbol{\psi}) \tag{A. 2}$$

This can be rewritten in the form

$$E = \sum_{n=1}^{N} \int_D \bar{\psi}_i(\boldsymbol{x})\, v_i^n(\boldsymbol{x}) d\boldsymbol{x} \int_D \bar{v}_j^n(\acute{\boldsymbol{x}})\, \psi_j(\acute{\boldsymbol{x}}) d\acute{\boldsymbol{x}}$$

$$E = \int_D \bar{\psi}_i(\boldsymbol{x}) \int_D \sum_{n=1}^{N} v_i^n(\boldsymbol{x}) \bar{v}_j^n(\acute{\boldsymbol{x}}) \psi_j(\acute{\boldsymbol{x}}) d\acute{\boldsymbol{x}}\, d\boldsymbol{x}.$$

For convenience, this will commonly be written as $E = (\boldsymbol{\psi}, \boldsymbol{K\psi})$ where the kernel, $K_{ij}$ is defined by

$$K_{ij}(\boldsymbol{x}, \acute{\boldsymbol{x}}) = \sum_{n=1}^{N} v_i^n\,(\boldsymbol{x}) \bar{v}_j^n(\acute{\boldsymbol{x}}) \tag{A. 3}$$

and the tensor product is defined by

$$K_{ij}\psi_j = \int_D K_{ij}(\boldsymbol{x}, \acute{\boldsymbol{x}}) \psi_j(\acute{\boldsymbol{x}})\, d\acute{\boldsymbol{x}} \tag{A. 4}$$

Unless otherwise stated, Einstein's summation convention is used throughout the equations. Now using the constraint $(\boldsymbol{\psi}, \boldsymbol{\psi}) = 1$ and introducing a Lagrange multiplier, λ, modified energy is introduced,

$$\mathrm{E}^*(\boldsymbol{\psi}) = (\boldsymbol{\psi}, \boldsymbol{K\psi}) - \lambda(\boldsymbol{\psi}, \boldsymbol{\psi})$$

Perturbing the eigenfunction slightly produces the equation

$$\mathrm{E}^*(\boldsymbol{\psi}+a\acute{\boldsymbol{\psi}}) = \int_D \overline{\psi_i + a\acute{\psi}_i} \int_D K_{ij}(\psi_j + a\acute{\psi}_j)\,\overline{d\acute{x}}d\bar{x} - \lambda \int_D \overline{\psi_i + a\acute{\psi}_i}\,(\psi_i + a\acute{\psi}_i)d\bar{x}$$

$$\mathrm{E}^*(\boldsymbol{\psi}+a\acute{\boldsymbol{\psi}}) = \int_D \overline{\psi_i + a\acute{\psi}_i} \int_D K_{ij}\psi_j\,\overline{d\acute{x}}d\bar{x} + \int_D \overline{\psi_i + a\acute{\psi}_i} \int_D K_{ij}a\acute{\psi}_i\,\overline{d\acute{x}}d\bar{x}$$

$$- \lambda \int_D \overline{\psi_i + a\acute{\psi}_i}\,\psi_i d\bar{x} + \int_D \overline{\psi_i + a\acute{\psi}_i}\,a\acute{\psi}_i d\bar{x}.$$

Minimizing in $a$ and $\bar{a}$ produces the equations

$$\frac{\partial}{\partial a}\mathrm{E}^*(\boldsymbol{\psi}+a\acute{\boldsymbol{\psi}})\Big|_{a=0=\bar{a}} = 0 = \int_D \int_D \bar{\psi}_i K_{ij}\acute{\psi}_j\,\overline{d\acute{x}}d\bar{x} - \lambda \int_D \acute{\psi}_i\acute{\psi}_j\,d\bar{x}$$

$$\frac{\partial}{\partial \bar{a}}\mathrm{E}^*(\boldsymbol{\psi}+a\acute{\boldsymbol{\psi}})\Big|_{a=0=\bar{a}} = 0 = \int_D \int_D \bar{\acute{\psi}}_i K_{ij}\psi_j\,\overline{d\acute{x}}d\bar{x} - \lambda \int_D \bar{\acute{\psi}}_i\psi_i\,d\bar{x}$$

$$\int_D \left[\int_D \psi_j K_{ij}\,d\bar{\acute{x}} - \lambda\psi_i\right]\bar{\acute{\psi}}_i\,d\bar{x} = 0.$$

Since $\acute{\psi}_i$ is arbitrary, this equation can only be true in the case

$$\int_D \psi_j(\acute{\boldsymbol{x}})K_{ij}(\boldsymbol{x},\acute{\boldsymbol{x}})\,d\bar{\acute{x}} - \lambda\psi_i(\boldsymbol{x}) = 0$$

$$\int_D K_{ij}(\boldsymbol{x},\acute{\boldsymbol{x}})\psi_j(\acute{\boldsymbol{x}})\,d\bar{\acute{x}} = \lambda\psi_i(\boldsymbol{x}) \qquad \text{(A. 5)}$$

This is the Eigenvalue problem commonly written as $\boldsymbol{K\psi} = \lambda\boldsymbol{\psi}$ using the product definition presented earlier. The solution of this problem will lead to the most energetic mode $\boldsymbol{\psi}(\boldsymbol{x})$ along with the energy in that mode $\lambda$.

## 2. Boundary Conditions

The physical velocity vectors used to form the eigenfunctions come from a flow satisfying the boundary conditions

$$v_i^n(x_1, 1) = v_i^n(x_1, -1) = 0.$$

The boundary condition for the eigenvectors which result from equation A.5 can be derived from applying the boundary conditions of equation A.6 to the original equation A.5 resulting in

$$\psi_i(x_1, 1) = \frac{1}{\lambda}\int_D K_{ij}(x_1, \acute{x}_1, 1, \acute{x}_2)\, \psi_j(\acute{x}_1, \acute{x}_2)\, d\bar{\boldsymbol{x}} \qquad \text{(A. 7)}$$

Using the definition of the kernel from equation A.3 produces the evaluations

$$K_{ij}(x_1, \acute{x}_1, 1, \acute{x}_2) = \sum_{n=1}^{N} v_i\,(x, 1)\bar{v}_j(\acute{x}_1, \acute{x}_2) = 0$$

$$K_{ij}(x_1, \acute{x}_1, -1, \acute{x}_2) = \sum_{n=1}^{N} v_i\,(x, -1)\bar{v}_j(\acute{x}_1, \acute{x}_2) = 0.$$

Simply applying these equations to equation A.7 results in the boundary conditions of the eigenfunctions

$$\psi_i(x_1, 1) = \int_D 0 \times \psi_j(\acute{x}_1, \acute{x}_2)\, d\bar{\acute{x}} = 0 \qquad \text{(A. 8)}$$

$$\psi_i(x_1, -1) = \int_D 0 \times \psi_j(\acute{x}_1, \acute{x}_2)\, d\bar{\acute{x}} = 0 \qquad (A.9)$$

So a set of eigenfunctions formed from a velocity field satisfying the no slip condition will themselves satisfy the no slip condition.

## 3. Incompressibility

Another property of the original flow field is in compressibility,

$$\frac{\partial}{\partial x_i} v_i(\boldsymbol{x}) = 0.$$

In order to evaluate the compressibility of the eigenfunctions' their divergence is taken from equation A.5 resulting in

$$\frac{\partial}{\partial x_i} \psi_i(\boldsymbol{x}) = \frac{1}{\lambda} \int_D \frac{\partial}{\partial x_i} K_{ij}(\boldsymbol{x}, \acute{\boldsymbol{x}})\, d\acute{\boldsymbol{x}}.$$

Noticing that the kernel is the only term in the integrand with a dependence on $x_i$ and using the definition of the kernel allows the application of the equation

$$\frac{\partial}{\partial x_i} K_{ij}(\boldsymbol{x}, \acute{\boldsymbol{x}}) = \sum_{n=1}^{N} \bar{v}_j(\acute{\boldsymbol{x}}) \frac{\partial}{\partial x_i} v_i(\boldsymbol{x}) = 0$$

to produce the divergence of the eigenfunctions

$$\frac{\partial}{\partial x_i} \psi_i(\boldsymbol{x}) = \int_D 0 \times \psi(\acute{\boldsymbol{x}})\, d\acute{\boldsymbol{x}} = 0 \qquad (A.10)$$

So the eigenfunctions formed from an incompressible velocity field are themselves incompressible.

## 4. Orthogonality

The eigenvalue equation produces multiple eigenfunctions and eigenvalues. Two solutions to the problem, $\boldsymbol{\psi^m}$ and $\boldsymbol{\psi^n}$ with corresponding eigenvalues $\lambda^m$, $\lambda^n$ satisfy of the equations

$$\int_D K_{ij}(\boldsymbol{x}, \acute{\boldsymbol{x}})\psi_j^m(\acute{\boldsymbol{x}})\, d\acute{\boldsymbol{x}} = \lambda^m\, \psi_i^m(\boldsymbol{x})$$

$$\int_D K_{ij}(\boldsymbol{x}, \acute{\boldsymbol{x}})\psi_j^n(\acute{\boldsymbol{x}})\, d\acute{\boldsymbol{x}} = \lambda^n\, \psi_i^n(\boldsymbol{x}).$$

Multiplying the first equation by $\bar{\boldsymbol{\psi}}^n(\boldsymbol{x})$ and integrating over the domain produces the equation

$$\lambda^m \int_D \psi_i^m(\boldsymbol{x})\bar{\psi}_i^n(\boldsymbol{x})d\boldsymbol{x} = \int_D \int_D K_{ij}(\boldsymbol{x}, \acute{\boldsymbol{x}})\psi_j^m(\acute{\boldsymbol{x}})\bar{\psi}_i^n(\boldsymbol{x})d\acute{\boldsymbol{x}}d\boldsymbol{x}$$

$$= \int_D \psi_j^m(\acute{\boldsymbol{x}}) \int_D K_{ij}(\boldsymbol{x}, \acute{\boldsymbol{x}})\bar{\psi}_i^n(\boldsymbol{x})d\boldsymbol{x}d\acute{\boldsymbol{x}}$$

$$= \int_D \psi_j^m(\acute{\boldsymbol{x}}) \int_D \overline{K}_{ij}(\acute{\boldsymbol{x}}, \boldsymbol{x})\bar{\psi}_i^n(\boldsymbol{x})d\boldsymbol{x}d\acute{\boldsymbol{x}}$$

$$= \lambda^n \int_D \psi_j^m(\acute{\boldsymbol{x}})\bar{\psi}_j^n(\acute{\boldsymbol{x}})d\acute{\boldsymbol{x}}.$$

Bringing both terms to the same side of the equation produces

$$(\lambda^m - \lambda^n) \int_D \psi_i^m(\boldsymbol{x})\bar{\psi}_i^n(\boldsymbol{x})d\boldsymbol{x} = 0.$$

Since $\lambda^m \neq \lambda^n$ for $m \neq n$ this equation can only be true if the functions are orthogonal,

$$\int_D \psi_i^m(\boldsymbol{x})\,\overline{\psi}_i^n(\boldsymbol{x})d\boldsymbol{x} = 0 \quad \text{for } m \neq n \tag{A.11}$$

The condition of orthogonality along with the constraint that the magnitude of each vector is 1 gives us the property of orthonormality $(\boldsymbol{\psi}^m, \boldsymbol{\psi}^n) = \delta_{mn}$ which simplifys the decomposition of a velocity field.

A velocity function can be written as a sum of eigenfunctions using the equation

$$v_i(\boldsymbol{x}, t) = \sum_m a_m(t)\psi_i^m(\boldsymbol{x}) \tag{A.12}$$

Multiplying both sides of the equation by $\overline{\boldsymbol{\psi}}^n(\boldsymbol{x})$ and integrating over the domain produces the equation

$$\int_D \overline{\psi}_i^n(\boldsymbol{x})v_i(\boldsymbol{x}, t)d\boldsymbol{x} = \sum_m a_m(t)\int_D \overline{\psi}_i^n(\boldsymbol{x})\psi_i^m(\boldsymbol{x})d\boldsymbol{x} \qquad = \sum_m a_m(t)\delta_{mn}$$

$$a_n(t) = \int_D \overline{\psi}_i^n(\boldsymbol{x})v_i(\boldsymbol{x}, t)d\boldsymbol{x} \tag{A.13}$$

Using this equation, the expansion coefficients $a_n(t)$ can easily be produced by integrating the product of the velocity and the conjugate of the eigenfunction. These coefficients can then be used to reconstruct the velocity field as seen in equation A.13.

## 5. Translational Invariance and Symmetry

The flow field for channel flow is both periodic and translationally invariant in the streamwise direction. As a result, any value can be added to the streamwise coordinate producing an equally valid velocity field which can be added to the original ensemble thereby increasing the size of the data set. To see how this affects the kernel $K_{ij}$ we add an arbitrary value $l$ to $x_1$ producing a new velocity field $v_i^n(x_1 + l, x_2)$. The original

kernel was the sum over all the independent time realizations $n$, so to include all possible velocity fields, the kernel is calculated from a sum over time and an integral over space

$$K_{ij} = \sum_{n=1}^{N} \int_0^{L_1} v_i^n(x_1 + l, x_2)\bar{v}_i^n(\acute{x}_1 + l, \acute{x}_2)\, dl.$$

Introducing a dummy variable $s = \acute{x}_1 + l$ along with the corresponding equations $x_1 + l = s + x_1 - \acute{x}_1$ and $dl = ds$ lets the kernel be written as

$$K_{ij} = \sum_{n=1}^{N} \int_{\acute{x}_1}^{\acute{x}_1 + L_1} v_i^n(x_1 - \acute{x}_1 + s, x_2)\bar{v}_j^n(s, \acute{x}_2)\, ds.$$

With the flow fields being periodic in the streamwise, direction, the limits of integration can be rewritten from 0 to $L_1$ and the integral can easily be seen to depend on only $x_1 - \acute{x}_1$ along with $x_2, \acute{x}_2$. Because the kernel is also periodic and translationally invariant in the spanwise direction the same analysis can be applied to that direction producing a kernel

$$K_{ij}(x_1 - \acute{x}_1, x_2, \acute{x}_2) = \sum_{n=1}^{N} \int_0^{L_1} v_i^n(x_1 - \acute{x}_1 + s_1, x_2) v_j^n(s_1, \acute{x}_2)\, ds \qquad \text{(A. 14)}$$

The original problem is now presented as

$$\int_0^{L_1} \int_{-1}^{1} K_{ij}(x_1 - \acute{x}_1, x_2, \acute{x}_2)\psi_j(\acute{x}_1, \acute{x}_2) d\acute{x}_2\, d\acute{x}_1 = \lambda\psi_i(x_1, x_2).$$

Multiplying both sides of the equation by $e^{-i\frac{2\pi m x_1}{L_1}}$ and integrating in the spanwise and streamwise directions produces the equation

$$\int_{-1}^{1} d\acute{x}_2 \int_0^{L_1} e^{-i\frac{2\pi m x_1}{L_1}} \psi_j(\acute{x}_1, \acute{x}_2) \int_0^{L_1} K_{ij}(x_1 - \acute{x}_1, \mathrm{x}_2, \acute{x}_2)\, e^{-i\frac{2\pi m x_1}{L_1}}\, dx_1\, d\acute{x}_1$$
$$= \lambda \int_0^{L_1} \psi_i(x_1, x_2) e^{-i\frac{2\pi m x_1}{L_1}}\, dx_1$$

which can be written as

$$\int_0^{L_1} \hat{\psi}_j(m, x_2)\hat{K}_{ij}(m, x_2, \acute{x}_2)d\acute{x}_2 = \lambda\hat{\psi}_i(m, x_2) \qquad \text{(A. 15)}$$

with the hat symbol denoting the Fourier transform of the kernel and the eigenfunction in the streamwise and spanwise directions.

A close examination of the transformed kernel $\hat{K}_{ij}$ shows how it can be calculated from the transform of the velocity vectors. Beginning with the definition of the kernel in equation A.14, multiplication by the exponentials and integration over the spanwise and streamwise direction yields

$$\hat{K}_{ij} = \sum_{n=1}^{N} \int_0^{L_1} \int_0^{L_1} v_i^n(x_1 - \acute{x}_1 + s_1, x_2) v_j^n(s_1, \acute{x}_2) e^{-i\frac{2\pi m x_1}{L_1}} dx_1\, ds_1.$$

Using a change of variables, $x_1^* = x_1 - \acute{x}_1 = s_1$ then splitting the exponents into two terms, produces

$$\hat{K}_{ij} = \sum_{n=1}^{N} \int_0^{L_1} \bar{v}_j^n(s_1, \acute{x}_2) e^{-i\frac{2\pi m x_1}{L_1}} \int_{-x_1+s_1}^{L_1-x_1+s_1} v_i^n(x_1^*, x_2) dx_1^*\, ds_1.$$

Note that the velocity is periodic in the streamwise direction so the integral can be written from $0$ to $L_1$and represent the Fourier transform of the velocity field in the streamwise direction $\hat{v}_i^n(m, x_2)$.

With the second integral having no dependence on $s_1$, the kernel is now the sum. The first integral can be rewritten as

$$\overline{\int_0^{L_1} \bar{v}_j^n(s_1, \acute{x}_2) e^{-i\frac{2\pi m x_1}{L_1}} ds_1} = \overline{\hat{v}_i^n}(m, \acute{x}_2).$$

Putting this all together, the transform of the kernel, $\widehat{K}_{ij}$ can then be calculated from a much simpler equation

$$\widehat{K}_{ij}(m, x_2, \acute{x}_2) = \sum_{n=1}^{N} \hat{v}_i^n(m, x_2)\, \overline{\hat{v}_j^n}(m, \acute{x}_2) \tag{A. 17}$$

Using the analysis, the decomposition must only be done in the wall normal direction on a kernel that has been transformed in the streamwise direction. The decomposition must be done for the Fourier mode $m$ producing a set of eigenfunctions denoted by their Fourier mode and quantum number $q$ written as $\hat{\psi}_i^q(m, x_2)$. The quantum number is an index to distinguish the various eigenvalues and eigenvectors ranging from 1, the most energetic mode to $N$, the least energetic mode.

The physical eigenfunctions are inverse Fourier transforms of these eigenfunctions $\hat{\psi}_i^q(m, x_2)$ so they have a sine and cosine dependence in the streamwise direction.

$$\hat{\psi}_i^{mq}(x_1, x_2) = \hat{\psi}_i^q(m, x_2) e^{-i\frac{2\pi m x_1}{L_1}}.$$

Both the position and the flow direction is being reversed in these directions so each of the new flow fields is physical satisfying boundary conditions, continuity and Navier Stokes Equations.

More specifically, with

$$\boldsymbol{v}^{n_1} = \langle v_1^{n_1}(x_1, x_2), v_2^{n_1}(x_1, x_2) \rangle$$

as an original flow field, new flow field can be obtained by symmetry

$$\hat{\boldsymbol{v}}^{n_2} = \left( v_1^{n_1}(x_1, -x_2), -v_2^{n_1}(x_1, -x_2) \right).$$

The Fourier transforms can be written in terms of the original transform as

$$\widehat{\boldsymbol{v}}^{n_2} = \left(\hat{v}_1^{n_1}(m, -x_2), -\hat{v}_2^{n_1}(m, -x_2)\right) \tag{A. 18}$$

By including these flow fields in the ensemble, the kernel takes the form

$$\widehat{K}_{ij}(m, x_2, \acute{x}_2) = \sum_{n=1}^{N} \sum_{p=1}^{2} \hat{v}_i^{np}(m, x_2)\, \overline{\hat{v}_j^{np}}(m, \acute{x}_2) \tag{A. 19}$$

The velocity is a physical quantity so it is also real. A property of the Fourier transform for physical variables is

$$\hat{v}_i(-m, x_2) = \overline{\hat{v}_i}(-m, x_2)$$

resulting in a similar property of the kernel

$$\widehat{K}_{ij}(-m, x_2) = \overline{\widehat{K}_{ij}}(-m, x_2).$$

Simply taking the complex conjugate of the equation A.15 leads to $\overline{\hat{\psi}_i}(-m, x_2)$ being the corresponding solution to $\widehat{K}_{ij}(-m, x_2)$ again having the same eigenvalue $\lambda$. If equation A.15 is solved for some Fourier mode $m > 0,$ an additional solution can be found for the wave number $-m$ and the energy in this mode is 2 times the energy of the reported eigenvalue. If the wave number is 0 then the energy reported is exactly equal to that of the eigenvalue. This factor of actual energy in a mode to eigenvalue is called degeneracy so an eigenfunction in the Fourier mode $m = 0$ has a degeneracy of 1, while an eigenfunction in the Fourier mode $m > 0$ has a degeneracy of 2.

The velocity fields in A.18 produce a set of relationships in a kernel that can be written as

$$\widehat{K}_{11}(m, x_2, -\acute{x}_2) = \widehat{K}_{11}(m, x_2, \acute{x}_2) \tag{A. 20a}$$

$$\widehat{K}_{12}(m, x_2, -\acute{x}_2) = -\widehat{K}_{12}(m, x_2, \acute{x}_2) \tag{A. 20b}$$

$$\widehat{K}_{22}(m, x_2, -\acute{x}_2) = \widehat{K}_{22}(m, x_2, \acute{x}_2) \tag{A. 20c}$$

The kernel needs to be computed in half of the domain, $x_2 \geq 0$ while the values in the other half of the domain are then obtained from these equations.

The time coefficients again come from the equation A.13. With two parameters needed to define the eigenfunctions, the same two parameters $m, q$ are needed to define the coefficients.

$$a_m^q(t) = \int_0^{L_1} \int_{-1}^{1} v_i(x_1, x_2, t) \hat{\psi}_i^q(m, x_2) e^{-i\frac{2\pi m x_1}{L_1}} dx_1\, dx_2 \tag{A. 21a}$$

$$a_m^q(t) = \int_{-1}^{1} \hat{v}_i(m, x_2, t) \overline{\hat{\psi}_i^q}(m, x_2)\, dx_2 \tag{A. 21b}$$